國立交通大學

電機與控制工程學系

博士論文

Bang-Bang 順滑控制在切換式電源轉換器之設計

Bang-Bang Sliding Mode Control in Switching Power Converters

研究生：蔡　建　峰

指導教授：陳　永　平　博士

中華民國九十六年十月

Bang-Bang 順滑控制在切換式電源轉換器之設計

Bang-Bang Sliding Mode Control in Switching Power Converters

研 究 生：蔡建峰　　Student：Jian-Feng Tsai

指導教授：陳永平　教授　　Advisor：Prof. Yon-Ping Chen

國 立 交 通 大 學

電機與控制工程學系

博 士 論 文

A Dissertation

Submitted to Department of Electrical and Control Engineering

College of Electrical and Computer Engineering

National Chiao-Tung University

in Partial Fulfillment of the Requirements

for the Degree of

Doctor of Philosophy

in

Electrical and Control Engineering

October 2007

Hsinchu, Taiwan, Republic of China

中華民國九十六年十月

Bang-Bang Sliding Mode Control in Switching Power Converters

Student: Jian-Feng Tsai Advisor: Yon-Ping Chen
Department of Electrical and Control Engineering
National Chaio-Tung University

Abstract

In this dissertation, the bang-bang sliding mode control is proposed to design the switching controller for a buck DC-DC converter. Normally, the on and off states of the switching device is modeled as an input switching between 1 and 0, and the reaching-and-sliding (RAS) regions are crucially related to the parameters of the sliding function. As a result, the sliding motions may not globally exist and different switching behaviors may be generated. With the bang-bang sliding mode control, the system trajectories of a buck DC-DC converter will clearly depicted in the phase plane and experimental results will be given for verifications. Besides, some considerations about the practical implementation are also included and a periodic ramp signal is added into the controller to achieve constant switching frequency. Then, the bang-bang sliding mode control is also adopted to design the switching controller for a class of switched systems. Two sufficient conditions to guarantee the existence of stable sliding motions will be given and the complex switching behaviors resulting from two switching functions will be clearly described. Moreover, the robustness of this switching controller to model uncertainties will be discussed. Finally, numerical simulations are given for demonstrations.

Bang-Bang 順滑控制在切換式電源轉換器之設計

研究生: 蔡建峰　　指導教授: 陳永平
國立交通大學
電機與控制工程學系

中文摘要

本論文利用 bang-bang 順滑控制來設計降壓式直流轉換電路之控制器，由於開關元件只操作在開和關兩個狀態，加上順滑迫近區間會因為選擇不同的順滑函數而改變，導致順滑行為無法全域地存在狀態空間中，並產生不同的切換行為。本論文會在相平面中詳盡地分析系統的狀態軌跡，同時經由實驗來驗證。此外，實務設計時所會面對的問題也將同時考量，並且加入週期性的斜坡函數來達到固定的切換頻率。最後，本論文將利用 bang-bang 順滑控制來設計某一類切換系統的控制器，同時提出存在穩定順滑行為的兩個條件，由於推導出的控制法則包含兩個切換函數，因此會產生複雜的切換行為，在本論文中也將清楚的描述這些切換行為，並更進一步探討該控制器對於系統中存在不確定模式的強健性，最後經由數值模擬來呈現。

致　　謝

本論文的完成，最得感謝 陳永平老師多年來的悉心指導，帶領我進入學術的殿堂與耐心的指導我論文寫作，並且讓我負責馬達組的研究，在此謹向老師表達最誠摯的感謝。同時，謝謝口試委員 徐國鎧老師、 鄭志強老師、 楊谷洋老師、 梁耀文老師與 張浚林老師的寶貴意見與指正，使本論文更臻於完善。

其次，謝謝世宏、倍榕與宗正在口試期間的幫忙，讓整個過程能夠順利進行。另外，謝謝馬達組的翰宏、欣達、思穎、胤宏與坤祐，由於你們的付出，讓研究能夠一點一滴的累積。對於可變結構實驗室的夥伴豐洲、桓展、子楊以及畢業的克聰學長、倉鴻、文魁和昌衢，也要說聲謝謝，因為有你們，研究生活才更加的多彩多姿。

最後，要感謝最親愛的父母親與姊姊，由於你們的體諒與支持，讓我能專心於課業，堅持到畢業這一刻，我愛你們。

Contents

List of Figure

List of Table

Chapter 1 Introduction

1.1 Research Motivation

The sliding mode control (SMC) is well known for its robustness to parameter variations and bounded matched disturbances [1-6]. With this advantage, the sliding mode control has been extensively applied to various fields of engineering applications, *e.g.*, robotic systems, electric drives and switching power converters [7-10]. The basic idea of the sliding mode control is enforcing the system trajectories to reach a predetermined sliding surface or sliding regime in a finite time and then stay on it thereafter. Once the sliding mode occurs, the controlled system will possess excellent robustness and invariance properties to the matched disturbance.

When the input only takes two possible values, it is called the bang-bang input, which originates from the optimal control and some examples can be found in [11]. While a bang-bang input is only available in the sliding mode control, it is referred to as the bang-bang sliding mode control. The major difference between it and the conventional sliding mode control is that the reaching-and-sliding (RAS) region may not be globally satisfied [12,13].

Switching power converters are the most significant systems with their control inputs only switching between 0 and 1. For the switched systems consisting of two subsystems, their inputs also take only two possible values of 1 and –1. Therefore, it is proper to design the switching controllers of these systems via bang-bang sliding mode control. This dissertation will mainly focus on the design of the switching controller for a buck DC-DC converter based on bang-bang sliding mode control and then apply it to stabilize the switched systems.

1.2 Sliding Mode in Switching Power Converters

A variety of SMC-based methods have been proposed for switching power converters [12,14-26]. Compared to the state-space average method [27,28], the sliding mode theory provides large signal stability and is more robust to uncertainties. Earlier, Sira-Ramirez presented detailed analyses about bilinear switched-networks and showed that based on the sliding mode theory, the output voltage regulation of a buck DC-DC converter could be achieved via indirect control with the exactly known model [12]. Then, Carpita and Marchesoni presented a robust sliding mode controller for the power conditioning system with resistive load variation and input disturbance; however, they didn't consider how the system performances are affected by different choice of the coefficients in sliding functions [17]. During that time, Spiazzi *et al.* proposed general purpose sliding mode control for DC-DC switching power converters [25,26]. More detailed analyses about the system stability were given and a simple method for switching power converters to operate at a constant switching frequency was proposed. Recently, Tan *et al.* give guidelines on the practical design of the sliding mode controller for buck DC-DC converters [19] and propose other SMC-based controllers to operate switching power converters at a constant switching frequency [20-22]. He and Luo also give another type of SMC-based controller to achieve constant switching frequency [23,24].

From above, there are mainly two purposes in these works. First, design a sliding function on which the system dynamics can be stabilized. For buck DC-DC converters, the simplest sliding function can be determined from the linear combination of state variables in the phase-variable control canonical form [17,19,25]. Other types of sliding functions are proposed by adding an integral term of the output

voltage error [20,24]. Second, modify the controllers such that switching power converters can operate at a constant switching frequency with the invariant property to input and load variations. Several possible methods have been proposed to achieve this objective [20,21,24,26]. Based on the equivalent control in the sliding mode, the duty cycle control signal of a PWM controller can be determined from the work of Tan *et al*. [20] and He and Luo [24]. An adjustable hysteresis band is proposed based on the adaptive feedforward and feedback control scheme in [21]. The adaptive feedforward loop is adopted to reduce the frequency deviation resulting from the input voltage variation. As for the adaptive feedback loop, it is used to adjust the parameter of the sliding function such that the frequency deviation resulting from the load variation can be eliminated. Another simple method is adding a periodic ramp signal into the hysteresis-type sliding mode controller and then using an additional PI-type compensator to reduce the steady-state error in the sliding mode [26]. Among these methods, the last one possesses the advantage of easier realization and preserves the original fast dynamic response in transient state. Therefore, this method will be adopted in this dissertation for the purpose of controlling the buck DC-DC converter at a constant switching frequency.

In switching power converters, their large-signal models depend on the different states of switching devices or diodes. Thus, large-signal multi-models should be adopted to describe the overall system dynamics and these switching power converters are treated as switched systems [29,30]. As a result, the stabilization problems in switched systems are very significant and worthy of research.

1.3 Stabilization Problems in Switched Systems

Switched systems are a special class of hybrid systems consisting of more than one subsystem [31]. Recently, more and more attentions have been paid to this filed and one of the most attractive problems is to stabilize the switched systems consisting of unstable subsystems (see, *e.g.*, [31-35] and the references cited therein). In the work of Wicks *et al.* [33,34], they incorporated the sliding mode theory to design the switching controllers for the switched systems with stable convex combinations of two subsystem matrices. In the work of Xu and Antsaklis [36], they discussed three classes of switched systems with subsystems possessing unstable foci, unstable nodes and saddle points. Their main idea is to choose an active subsystem such that the distance of the state to the origin is minimized, where the switching criterions are based on the angles of the subsystem vector fields and the geometric properties of the phase plane. In [37], Bacciotti proposed another stabilizing switching rule based on the damping feedback originated from the work by Jurdjevic and Quinn [38]. In his later work with Ceragioli [39], a state-static-memoryless stabilizing feedback law was proposed to stabilize a different class of switched systems, in which one of the subsystems has a pair of conjugate imaginary eigenvalues. Recently, Lin and Antasklis consider a class of uncertain switched systems satisfying the assumptions that their subsystems contain stable auxiliary systems and there exist no unstable sliding motions [40]. Motivated by the works of Wicks *et al.* [33,34], this dissertation will extend the bang-bang sliding mode control to design the switching controller for another class of switched systems. Compared with their work, we will give more theoretical analyses about the sliding motions in the switched systems and provide two important assumptions to guarantee the existence of stable sliding motions.

1.4 Organization of the Dissertation

The remaining contents of this dissertation are organized as follows. In Chapter 2, the fundaments of the sliding mode theory are given as preliminaries and then the properties of the bang-bang sliding mode control are discussed. In Chapter 3, the switching controller of a buck DC-DC converter is designed based on the bang-bang sliding mode control. The switching behaviors will be analyzed in the phase plane and experiment results will be given for verifications. Some practical considerations will also be included and the original controller will be modified to achieve constant switching frequency by adding a periodic ramp signal. In Chapter 4, the bang-bang sliding mode control is extended to design the switching controller for a class of switched systems and two important assumptions to guarantee the existence of stable sliding motions will be given. Moreover, it will show that the switching control laws consist of two switching functions and the complex switching behaviors will be clearly described. Further, the robustness of this switching controller to the model uncertainties will be discussed. Finally, conclusions and suggestions for future research are given in Chapter 5.

Chapter 2 Bang-Bang Sliding Mode Control

In this chapter, the basic sliding mode theory is first introduced in §2.1 as preliminaries. Then, the problem resulting from the fixed input and the existence condition of sliding motion will be presented. Finally, the features of the bang-bang sliding mode control are discussed and three modes of the switching behaviors near the switching surface are described in §2.2.

2.1 Preliminaries of General Sliding Mode Control

Generally, there are two fundamental steps to design a sliding mode control. First, choose an appropriate sliding surface or sliding manifold $\boldsymbol{s}$ to guarantee the system stability in the sliding mode $\boldsymbol{s}=\boldsymbol{0}$. Second, derive the control algorithm such that the system trajectories can reach the sliding surface in a finite time and then stay thereafter [1-6]. For example, consider a linear time invariant system expressed as

$$\dot{\boldsymbol{x}} = \boldsymbol{A}\boldsymbol{x} + \boldsymbol{B}\boldsymbol{u} + \boldsymbol{B}\boldsymbol{h}(\boldsymbol{x},t) \tag{2.1}$$

where $\boldsymbol{A}$ is the $n\times n$ system matrix, $\boldsymbol{B}$ is the $n\times m$ input matrix, $\boldsymbol{x}$ is the $n\times 1$ state vector, $\boldsymbol{u}$ is the $m\times 1$ input vector and $\boldsymbol{h}$ is the $m\times 1$ matched input disturbance. Without loss of generality, the pair $(\boldsymbol{A},\boldsymbol{B})$ is assumed to be controllable and $\boldsymbol{B}$ is of full rank.

In the first step, the sliding surface is selected as

$$\boldsymbol{s} = \boldsymbol{C}\boldsymbol{x} \tag{2.2}$$

where $\boldsymbol{s}=[s_1,s_2,\ldots,s_m]^T$ and $\boldsymbol{C}$ is a $m\times n$ coefficient matrix. Note that the choice of $\boldsymbol{C}$ must guarantee the existence of stable sliding motions and several approaches have been proposed, *e.g.*, the transformation matrix method [41], the eigenstructure assignment method [42] and the Lyapunov-based method [43]. Then, design the input $\boldsymbol{u}=[u_1\ u_2\ \ldots\ u_m]$ by discontinuous feedback, where

$$u_i = \begin{cases} u_i^+(\boldsymbol{x}), & s_i(\boldsymbol{x}) > 0 \\ u_i^-(\boldsymbol{x}), & s_i(\boldsymbol{x}) < 0 \end{cases}, \quad i = 1,2,\ldots,m \tag{2.3}$$

With the control algorithm (2.3), the reaching-and-sliding (RAS) condition must be satisfied by

$$s_i \dot{s}_i < -\sigma_i |s_i|, \qquad s_i \neq 0 \tag{2.4}$$

where σ_i are positive. Once (2.4) is satisfied, the system trajectories could reach the sliding mode $\boldsymbol{s}=\boldsymbol{0}$ in a finite time and then stay thereafter [1].

Next, consider a single input bilinear system [11] expressed as

$$\dot{\boldsymbol{x}} = \boldsymbol{f}(\boldsymbol{x}) + u\boldsymbol{g}(\boldsymbol{x}) + \boldsymbol{h}(\boldsymbol{x},t) \tag{2.5}$$

where $\boldsymbol{f}$ and $\boldsymbol{g}$ are both $n\times 1$ vector functions and $\boldsymbol{h}$ is a $n\times 1$ external disturbance vector. While the sliding mode occurring, the following invariance conditions [12] are satisfied

$$s = 0 \quad \text{and} \quad L_{\boldsymbol{f}+u\boldsymbol{g}+\boldsymbol{h}} s = 0 \tag{2.6}$$

where $L_{\boldsymbol{f}+u\boldsymbol{g}+\boldsymbol{h}} s$ denotes the directional derivative of the scalar function s with respect to the vector filed $\boldsymbol{f}+u\boldsymbol{g}+\boldsymbol{h}$. Then, the equivalent control u_{eq} can be defined as

$$u_{eq}(x) = -\frac{L_{f+h} s}{L_g s} \tag{2.7}$$

Theoretically, the ideal sliding dynamics or equivalent system dynamics can be obtained by substituting u_{eq} into (2.5). However, there exist two considerable problems in (2.7). First, u_{eq} must satisfy the intermediate condition [14], *i.e.*, u_{eq} must be bounded by

$$min(u^+, u^-) < u_{eq}(x) < max(u^+, u^-) \tag{2.8}$$

Therefore, RAS-condition can only be satisfied in the region determined from (2.8), which is referred to as the reaching-and-sliding (RAS) region [13]. Second, the existence of sliding motion on s is guaranteed if the transversality condition [12] is satisfied by

$$L_g s \neq 0 \tag{2.9}$$

For the linear time invariant system (2.1), it is easy to satisfy the transverality

condition by choosing a $\boldsymbol{C}$ such that the $m \times m$ square matrix $\boldsymbol{CB}$ is invertible, *i.e.*, $(\boldsymbol{CB})^{-1}$ exists. However, for bilinear systems, the state variables are involved in $\boldsymbol{g}(\boldsymbol{x})$ and thus, (2.9) may not be satisfied in some region, in which the stability can not be guaranteed.

2.2 Properties of Bang-Bang Sliding Mode Control

In this dissertation, the sliding mode theory is applied to the systems with the input only switching between two fixed values, which is referred to as bang-bang sliding mode control. With the constrained input, the RAS-condition may not be globally satisfied and thus the system trajectories will not slide along $s=0$ outside the RAS-region. Generally, the switching behaviors around $s=0$, as shown in Fig. 2.1, can be classified into three following modes [44]:

1. Refractive mode: the system trajectories are directed toward $s=0$ on one side and away from $s=0$ on the other side.
2. Attractive mode: the system trajectories are directed toward $s=0$ on both sides.
3. Rejective mode: the system trajectories are directed away from $s=0$ on both sides.

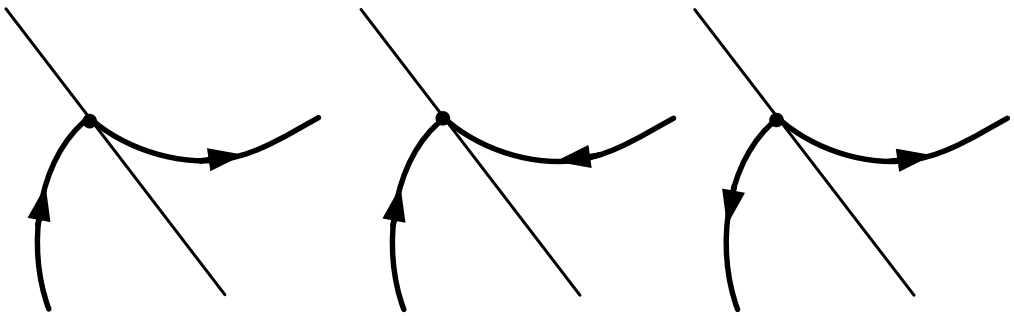

Fig. 2.1 Three modes of switching behaviors on $s=0$.

(a) Refractive mode. (b) Attractive mode. (c) Rejective mode.

Mathematically, these switching modes can be represented by following equations:

$$\dot{s}(\boldsymbol{x})\big|_{u=u^+} \cdot \dot{s}(\boldsymbol{x})\big|_{u=u^-} > 0 \text{ on } s(\boldsymbol{x}) = 0 \tag{2.10}$$

for the refractive mode,

$$s(\boldsymbol{x}) \cdot \dot{s}(\boldsymbol{x}) < 0 \qquad \text{around } s(\boldsymbol{x}) = 0 \tag{2.11}$$

for the attractive mode, and

$$s(\boldsymbol{x}) \cdot \dot{s}(\boldsymbol{x}) > 0 \qquad \text{around } s(\boldsymbol{x}) = 0 \tag{2.12}$$

for the rejective mode. Obviously, the attractive mode on $s(\boldsymbol{x})=0$ is the sliding mode. In switching power converters, if they can be stabilized by the sliding mode control, only refractive mode and attractive mode will occur on $s(\boldsymbol{x})=0$. Usually, they are designed to operate only in the attractive mode (*i.e.*, the sliding mode), and slide on it thereafter. Sometimes, they may be designed to operate from refractive mode to attractive mode purposely for achieving faster system dynamics.

In next chapter, it will show that there exist only refractive mode and attractive mode around the sliding function in the buck DC-DC converter. The system trajectories will be clearly depicted in the phase plane and verified by experimental results. In Chapter 4, the switching behaviors in switched systems will be more complicated since the derived switching control laws consist of two switching functions: one is the predetermined sliding function and the other one is the switching boundary resulting from the bilinear model of switched systems. It will show that only attractive mode will occur around the sliding function but all three switching modes may exist around the other switching boundary. Besides, there may exist unstable hyper-switching motion around the intersection of these two switching functions in high-order switched systems. This complicated switching phenomenon will be briefly discussed in Chapter 5 as our future research.

Chapter 3 Bang-Bang Sliding Mode Control in Switching Power Converters

With the switching property, the sliding mode theory provides an intuitive way to control switching power converters [12,15]. Compared with the state-space average method [27,28], the sliding mode theory leads to large signal stability. Besides, it is robust to uncertainties and much easier for the implementation.

For simplicity, a buck DC-DC converter is conventionally modeled as a linear system by neglecting the unknown parasitic resistance, which usually results in a small uncertain variation and then reduces the system precision. For improvement, the unknown parasitic resistance is taken into consideration, which makes the buck DC-DC converter modeled as an uncertain bilinear system. However, it is not easy to deal with such an uncertain bilinear model by conventional control technologies.

Generally, most of the existing works are based on the assumption that the buck DC-DC converter operates only in the continuous conduction mode (CCM). However, if the components' values are not appropriately selected, the buck DC-DC converter may operate in the discontinuous conduction mode (DCM). In this chapter, it will show that the buck DC-DC converter can be finally driven into the predetermined sliding mode regardless of the existence of DCM during the transient state.

The remainder of this chapter is organized as follows. In §3.1, the model of a buck DC-DC converter with parasitic resistance is first introduced as an uncertain bilinear system. Then, it is modified as a linear system in the phase-variable control canonical form. In §3.2, the design procedures of bang-bang sliding mode control will be given and the system trajectories with different switching behaviors will be clearly depicted

in the phase plane. Then, experimental results of the buck DC-DC converter subject to load variation and different choices of sliding functions will be demonstrated in §3.3. Finally, some considerations about the practical implementation and the method of operating the switching power converters at a constant switching frequency will be included in §3.4.

3.1 Model Description of Buck DC-DC Converter

A buck DC-DC converter with resistive load is illustrated in Fig. 3.1, where E is the DC voltage source, L is the inductor, C is the capacitor, i_L is the inductor current, i_C is the capacitor voltage, v_o is the output voltage, D is the diode, S is the switching device, R is the resistive load and r_d is the unknown parasitic resistance in the circuit. Note that $R=R_0+\Delta R$, where R_0 is the nominal value of resistive load and ΔR varies in the range of $[\delta r_1, \delta r_2]$. Clearly, $R\in[R_{\min},R_{\max}]$, where $R_{\min}=R_0+\delta r_1$ and $R_{\max}=R_0+\delta r_2$.

Assume that the buck DC-DC converter operates in CCM. Then, the state-space equation can be expressed as

$$\begin{bmatrix}\dot{i}_L\\ \dot{v}_C\end{bmatrix}=\begin{bmatrix}0 & -\frac{1}{L}\\ \frac{1}{C} & -\frac{1}{RC}\end{bmatrix}\begin{bmatrix}i_L\\ v_C\end{bmatrix}+\begin{bmatrix}-\frac{r_d}{L} & 0\\ 0 & 0\end{bmatrix}\begin{bmatrix}i_L\\ v_C\end{bmatrix}u+\begin{bmatrix}\frac{E}{L}\\ 0\end{bmatrix}u \qquad (3.1)$$

where u represents the on state and off state of the switching device S by the values of 1 and 0. Note that (3.1) is linear in control and linear in state variables i_L and v_C, but not jointly linear in control and state variables. That means (3.1) is a bilinear system [11].

Now, let the desired output voltage be a constant V_d. Define v_o-V_d and i_C/C as the new state variables x_1 and x_2. Then, we have

$$\dot{x}_1=d(v_o-V_d)/dt=dv_o/dt=i_C/C=x_2 \qquad (3.2)$$

Note that v_o is equivalent to v_C if the equivalent serial resistance (ESR) of C is

neglected. From Fig. 3.1, it is easy to obtain that

$$i_L = i_C + v_o/R = Cx_2 + (x_1 + V_d)/R \tag{3.3}$$

Further differentiating (3.3) and using the first equation in (3.1), it leads to

$$\dot{x}_2 = -\frac{1}{LC}x_1 - \frac{1}{RC}x_2 + \frac{E}{LC}u - \frac{r_d}{LC}i_L u - \frac{V_d}{LC} \tag{3.4}$$

Let $\boldsymbol{x}$ be $[x_1\ x_2]^T$, (3.2) and (3.4) could be rewritten as

$$\dot{\boldsymbol{x}} = \boldsymbol{A}\boldsymbol{x} + (\boldsymbol{B} + \Delta\boldsymbol{B}(\boldsymbol{x}))u + \boldsymbol{h} \tag{3.5}$$

where

$$\boldsymbol{A} = \begin{bmatrix} 0 & 1 \\ -\frac{1}{LC} & -\frac{1}{RC} \end{bmatrix} \tag{3.6}$$

$$\boldsymbol{B} = \begin{bmatrix} 0 \\ \frac{E}{LC} \end{bmatrix} \tag{3.7}$$

$$\Delta\boldsymbol{B}(\boldsymbol{x}) = \begin{bmatrix} 0 \\ -\frac{r_d i_L}{LC} \end{bmatrix} = \begin{bmatrix} 0 \\ -\frac{r_d}{RLC}x_1 - \frac{r_d}{L}x_2 - \frac{r_d V_d}{RLC} \end{bmatrix} \tag{3.8}$$

$$\boldsymbol{h} = \begin{bmatrix} 0 \\ -\frac{V_d}{LC} \end{bmatrix} \tag{3.9}$$

Significantly, the bilinear system (3.1) is changed into (3.5), which is a linear system with control input u and encounters the state-dependent uncertainty $\Delta\boldsymbol{B}(\boldsymbol{x})$ and external input $\boldsymbol{h}$. Since both $\Delta\boldsymbol{B}(\boldsymbol{x})u$ and $\boldsymbol{h}$ are matched disturbances, it is suitably to design the controller with the sliding mode control technique.

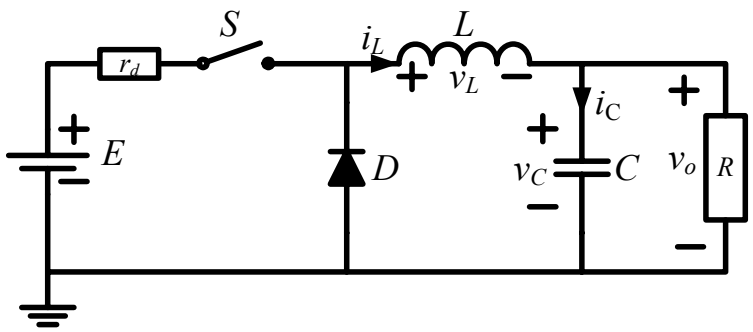

Fig. 3.1 Buck DC-DC converter with resistive load.

3.2 Design Procedures and Phase Plane Analysis

In this section, the design procedures of bang-bang sliding mode control for a buck DC-DC converter are introduced first. Then, the RAS-regions will be shown to crucially relate to the coefficients of sliding functions. Finally, the system trajectories with different sliding functions will be clearly depicted in the phase plane.

3.2.1 Design Procedures of Bang-Bang Sliding Mode Control

In general, there are two fundamental steps to design a sliding mode control. First, choose an appropriate sliding function s to guarantee the system stability in the sliding mode s=0. Second, derive the control algorithm such that the system trajectories can reach the sliding surface in a finite time and then stay on s=0 thereafter. However, unlike the conventional sliding mode control, the control input u in (3.5) only switches between 1 and 0, which makes the controller design more restrictive.

In the first step, let the sliding function or sliding line be chosen as

$$s = x_2 + \lambda x_1 \tag{3.10}$$

where λ is a positive constant. Obviously, it will guarantee that the system dynamics is stable in the sliding mode s=0 since the system is represented in the phase-variable control canonical form. For the second step, the bang-bang sliding mode control algorithm is purposely designed as

$$u = 0.5\left(1 - sgn\left(s\right)\right) \tag{3.11}$$

which switches between 1 and 0 depending on the scalar sign of s. Most importantly, (3.11) must satisfy the following RAS-condition:

$$s\dot{s} < 0\ ,\ \forall s \neq 0 \tag{3.12}$$

such that the system trajectories will reach the sliding line, but may be not in a finite time, and then stay thereafter. From (3.5) and (3.10), the derivative of the sliding function with respect to time is

$$\dot{s} = -\frac{1}{LC}x_1 + \left(\lambda - \frac{1}{RC}\right)x_2 + \frac{E}{LC}u - \frac{r_d}{LC}i_L u - \frac{V_d}{LC} \tag{3.13}$$

Further substituting the control input (3.11) into (3.13), it leads to

$$\dot{s} = \begin{cases} -\frac{1}{LC}x_1 + \left(\lambda - \frac{1}{RC}\right)x_2 + \frac{E - r_d i_L}{LC} - \frac{V_d}{LC} & \text{for } s < 0 \\ -\frac{1}{LC}x_1 + \left(\lambda - \frac{1}{RC}\right)x_2 - \frac{V_d}{LC} & \text{for } s > 0 \end{cases} \tag{3.14}$$

If the following inequality is satisfied

$$\frac{V_d}{LC} - \frac{E - r_d i_L}{LC} < -\frac{1}{LC}x_1 + \left(\lambda - \frac{1}{RC}\right)x_2 < \frac{V_d}{LC} \tag{3.15}$$

the RAS-condition (3.12) is guaranteed. The region described by the inequality (3.15) is the RAS-region. Replacing i_L by (3.3), (3.15) can be rewritten into two inequalities as

$$\begin{cases} \frac{(R+r_d)V_d - RE}{RLC} < -\frac{(R+r_d)}{RLC}x_1 + \left(\lambda - \frac{1}{RC} - \frac{r_d}{L}\right)x_2 \\ -\frac{1}{LC}x_1 + \left(\lambda - \frac{1}{RC}\right)x_2 < \frac{V_d}{LC} \end{cases} \tag{3.16}$$

Clearly, the RAS-region must be determined from s and two lines, l_1 and l_2, with the slopes being $m_1=(R+r_d)/(RLC\lambda-L-RCr_d)$ and $m_2=R/(RLC\lambda-L)$ respectively. Since m_1 and m_2 are related to the values of components in the buck DC-DC converter and λ, the relations among l_1, l_2 and s can be classified into six cases: "A, B, C, D, E, F" as listed in Table 3.1 and they are also plotted in Fig. 3.2. Note that $\mathbf{P}_1((RV_d+r_dV_d-RE)/(R+r_d),0)$ and $\mathbf{P}_2(-V_d,0)$ are the crossing points of l_1 and l_2 in x_1-axis.

Table 3.1 The relations among l_1, l_2 and s.

Case	λ	m_1, m_2
A	$0<\lambda\leq 1/RC-R/L$	$m_1<0$, $m_2<0$, $m_1\leq m_2<-\lambda$ $(L/C>R^2)$
B	$1/RC-R/L<\lambda<1/RC$	$m_1<0$, $m_2<0$, $m_2<m_1<-\lambda$
C	$\lambda=1/RC$	$m_1<0$, $m_2=\infty$, $m_1<-\lambda<m_2$
D	$1/RC<\lambda<1/RC+r_d/L$	$m_1<0$, $m_2>0$, $m_1<-\lambda<m_2$
E	$\lambda=1/RC+r_d/L$	$m_1=\infty$, $m_2>0$, $-\lambda<m_2< m_1$
F	$1/RC+r_d/L<\lambda$	$m_1>0$, $m_2>0$, $-\lambda<m_2< m_1$

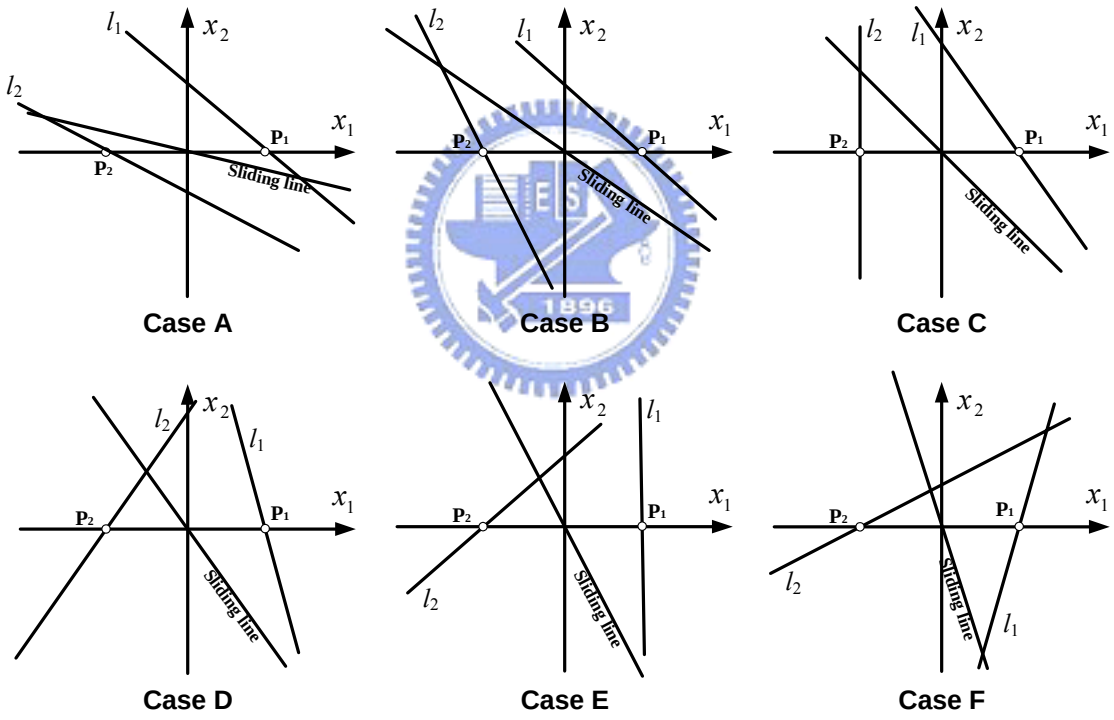

Fig. 3.2 Six cases with l_1, l_2 and s in the phase plane.

3.2.2 Phase Plane Analysis

In normal operation, the output voltage v_o of a buck DC-DC converter is nonnegative, which implies

$$x_1 = v_o - V_d \geq -V_d \tag{3.17}$$

and then the system trajectories should be inherently in the right-half plane of $x_1=-V_d$. Moreover, when a buck DC-DC converter operates in CCM, i_L should be larger than zero and (3.3) can be consequently rewritten as

$$i_C(t) > -\frac{v_o(t)}{R} \tag{3.18}$$

While the components of the buck DC-DC converter are not well designed, it may operate in DCM with $i_L=0$ and the system dynamics is governed by

$$i_C(t) = -\frac{v_o(t)}{R} \tag{3.19}$$

Since $x_1=v_o-V_d$ and $x_2=i_C/C$, (3.18) and (3.19) can be rewritten as

$$x_1 + RCx_2 > -V_d \tag{3.20}$$

and

$$x_1 + RCx_2 = -V_d \tag{3.21}$$

Note that the linear function (3.21) is referred to as the drifting line in this dissertation. According to (3.17), (3.20) and (3.21), the system trajectories of a buck DC-DC converter should be restricted to the region:

$$\Omega = \begin{cases} x_1 \geq -V_d \\ x_1 + RCx_2 \geq -V_d \end{cases} \tag{3.22}$$

as shown in Fig. 3.3, where the system trajectories with different initial conditions are also included for $u=0$(dashed line) and $u=1$ (solid line). The system trajectories depicted by dashed line and solid line will converge to $Q_1(-V_d,0)$ and $Q_2(E-V_d,0)$ respectively. All the system trajectories with $u=0$ move clockwise to reach the drifting line first and then approach Q_1. As for the system trajectories with $u=1$, they move spirally clockwise to Q_2.

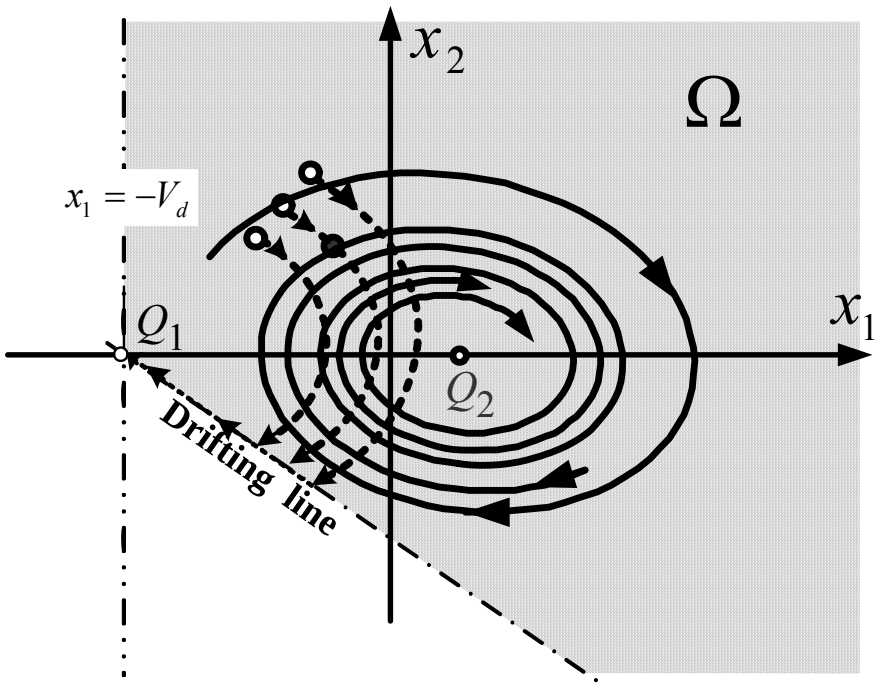

Fig. 3.3 System trajectories with different initial conditions.

According to Table 3.1, the RAS-regions could be mainly classified into two types: $\lambda \leq 1/RC$ as Type-I and $\lambda > 1/RC$ as Type-II. Clearly, Type-I consists of case A, case B and case C and Type-II consists of case D, case E and case F. For Type-I, Ω is the RAS-region and separated into Ω_0 and Ω_1 by s=0, as depicted in Fig. 3.4. From (3.16), Ω_0 and Ω_1 are bounded as

$$\Omega_0 = \begin{cases} s > 0 \\ l_2 < 0 \\ x_1 > -V_d \\ x_1 + RCx_2 > -V_d \end{cases}, \text{ for } u = 0 \tag{3.23}$$

$$\Omega_1 = \begin{cases} s < 0 \\ l_1 > 0 \\ x_1 > -V_d \\ x_1 + RCx_2 > -V_d \end{cases}, \text{ for } u = 1 \tag{3.24}$$

Two system trajectories related to J_0 in Ω_0 and J_1 in Ω_1 are also shown in Fig. 3.4, where J_0 and J_1 represent the initial conditions. Since all the system trajectories in Ω_0 and Ω_1 satisfy the RAS-condition (3.12), the system trajectories starting from J_0 and

J_1 will approach the sliding line and then generate the desired sliding mode s=0. From (3.10), the system dynamics will be exponentially stable in the sliding mode.

Obviously, the RAS-condition is globally satisfied in Ω for the cases of Type-I and the system trajectories will never enter the drifting line. Thus, if the following inequality is satisfied

$$\lambda \le 1/RC \tag{3.25}$$

all the switching behaviors around s=0 are exactly of the attractive mode as discussed in §2.2, and the buck DC-DC converter will operate only in CCM. Typically, λ will be chosen as $1/RC$ such that the RAS-region is large enough [19]. However, the system dynamics with $\lambda = 1/RC$ may be too slow if faster response is required during the start-up or in the transient state.

As for the cases of Type-II, the switching behaviors are more complicated than the cases of Type-I, due to the RAS-condition is only locally satisfied in Ω. From (3.16), four sub-regions, Ω_0, Ω'_0, Ω_1 and Ω'_1, as shown in Fig. 3.5, can be obtained and they are bounded as

$$\Omega_0 = \begin{cases} s > 0 \\ l_2 < 0 \\ x_1 > -V_d \\ x_1 + RCx_2 > -V_d \end{cases}, \text{ for } u = 0 \tag{3.26}$$

$$\Omega'_0 = \begin{cases} s > 0 \\ l_2 > 0 \\ x_1 > -V_d \end{cases}, \text{ for } u = 0 \tag{3.27}$$

$$\Omega_1 = \begin{cases} s < 0 \\ l_1 > 0 \\ x_1 > -V_d \\ x_1 + RCx_2 > -V_d \end{cases}, \text{ for } u = 1 \tag{3.28}$$

$$\Omega'_1 = \begin{cases} s < 0 \\ l_1 < 0 \\ x_1 + RCx_2 > -V_d \end{cases}, \text{ for } u = 1 \tag{3.29}$$

where Ω_0 and Ω'_0 are related to u=0 and Ω_1 and Ω'_1 are related to u=1. There are

mainly five kinds of system trajectories shown in Fig. 3.5, corresponding to five different points J_0, J_1, J_2, J_3 and J_4. For the system trajectories through J_0 and J_1, they are just like the cases of Type-I, which will reach the sliding line. For the system trajectory through J_2, it may come from Ω_1 or start from Ω'_0. From Fig. 3.5, this system trajectory will enter the sub-region Ω_0. For the system trajectory through J_3, it may come from Ω_0 or start from Ω'_1. Also viewing from Fig. 3.5, this system trajectory will enter the sub-region Ω_1. Finally, for the system trajectory through J_4, it comes from Ω'_0 and then moves along the drifting line with u=0. Once this system trajectory passes through the sliding line, it will move into the sub-region Ω'_1, where u is changed from 0 to 1. According to the trends of these five system trajectories, all of them will be eventually reach the segment, between $\mathbf{S}_1$ and $\mathbf{S}_2$ of the sliding line and then slide along it to the origin. Compared with the cases of Type-I, the system trajectories of Type-II may include DCM in the transient state, but they can still be successfully driven into the sliding line and kept on s=0 with a larger convergent rate. Obviously, it corresponds to the discussion in §2.2 that the switching power converters will possess faster dynamic response while they are operated from refractive mode to attractive mode.

From the above analyses, the bang-bang sliding mode control is shown to be an effective method to drive all the system trajectories to reach the sliding line and then converge to the origin, *i.e.*, the output voltage regulation of the buck DC-DC converter is theoretically achieved. In next section, several experiments will be conducted to verify the proposed bang-bang sliding mode control.

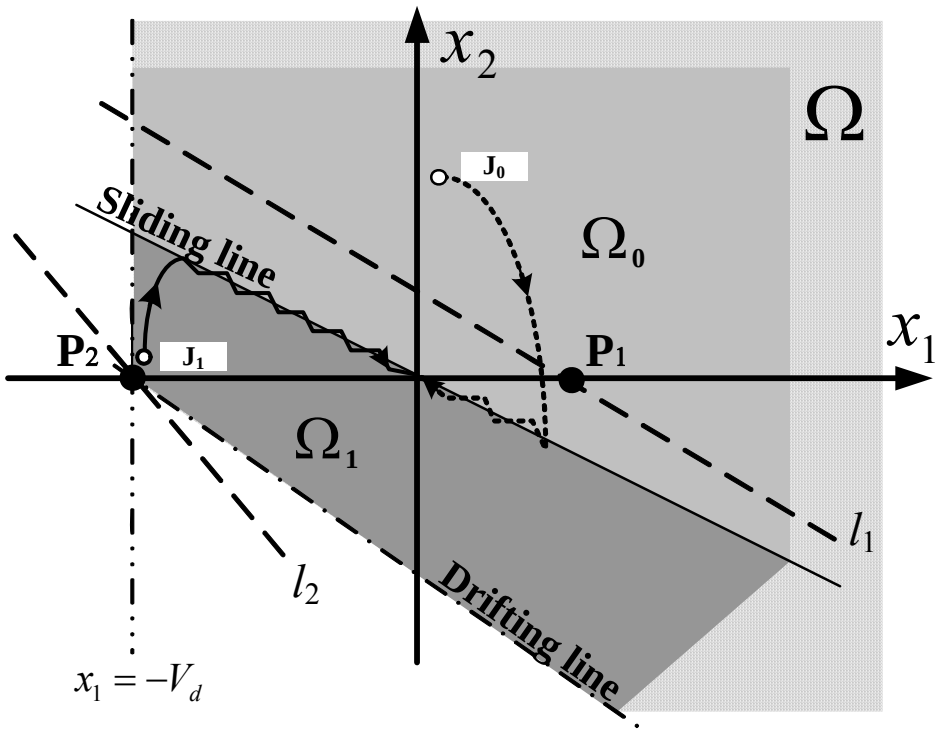

Fig. 3.4 System trajectories in the cases of Type-I.

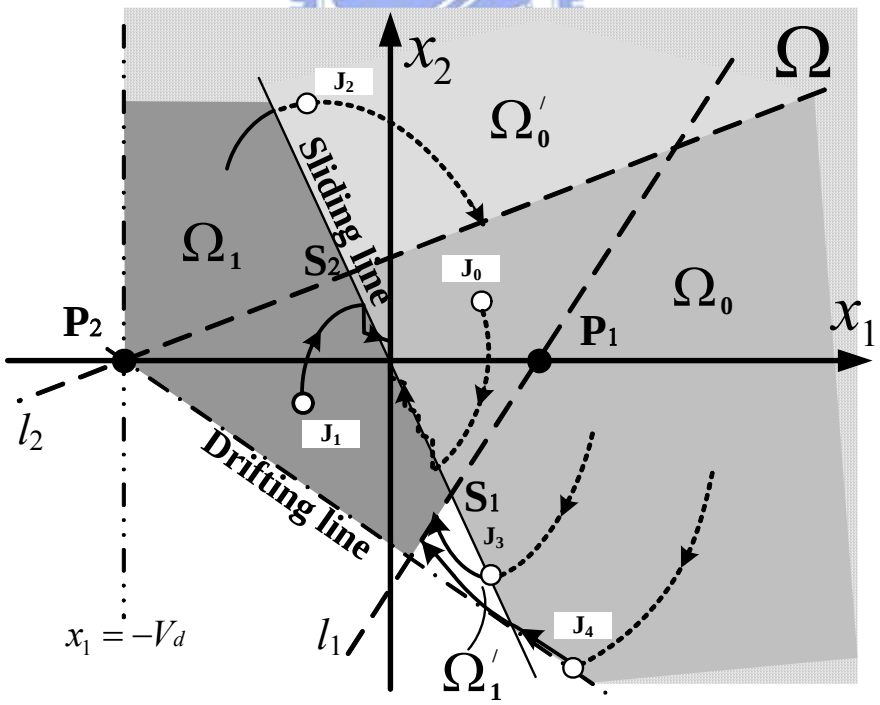

Fig. 3.5 System trajectories in the cases of Type-II.

3.3 Experimental Results

A lab-prototype of buck DC-DC converter for theoretically verifying is fabricated as shown in Fig. 3.6, in which s_g denotes the gate driver signal, i_C is the sensed capacitor current, v_o is the sensed output voltage, and a PC-based controller is used to implement the bang-bang sliding mode control. The maximum sampling rate is limited at 20kHz and the parameters of the buck DC-DC converter are listed in Table 3.2. In the following examples, it will show the performances of the bang-bang sliding mode control in output voltage regulation subject to different sliding functions and load variations.

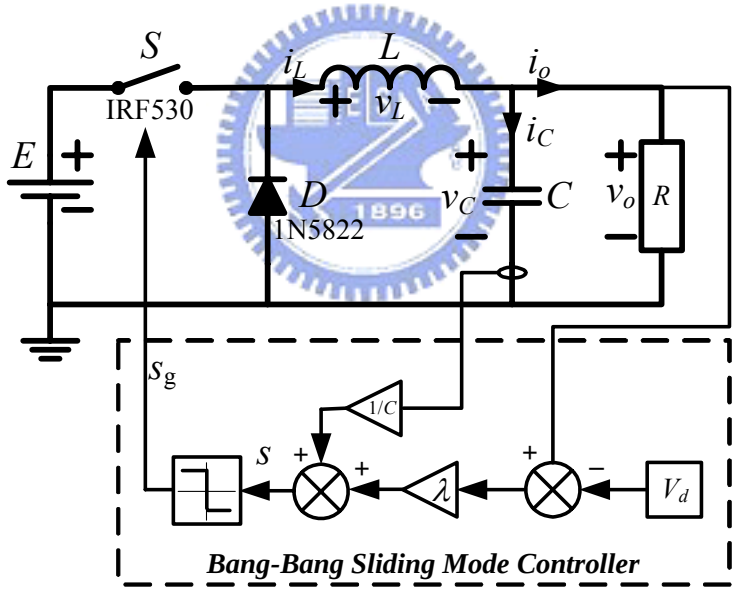

Fig. 3.6 The bang-bang sliding mode controller for the buck DC-DC converter.

Table 3.2 Parameters of the buck DC-DC converter.

Parameter	E	L	C	R	V_d
Value	12.28(V)	2.47(mH)	470(μF)	15.35(Ω)	8(V)

Example 3.1:

The experimental results shown in Fig. 3.7, Fig. 3.8 and Fig. 3.9 are obtained by choosing three different sliding functions with λ=100, λ=500 and λ=1000. All the system trajectories are all successfully driven to the corresponding sliding lines and then move toward the origin, as shown in Fig. 3.7. For the system trajectory with λ=100, it corresponds to the case of Type-I that goes through J_1. As for the system trajectories with λ=500 and 1000, they correspond to the case of Type-II that goes through J_1. Note that $1/RC$=141.8 and thus the case with λ=100 is of Type-I, and the cases with λ=500 and 1000 are of Type-II. From Fig. 3.8, it is easy to find that the system trajectories with smaller λ will reach the sliding line faster than those with larger λ. However, from Fig. 3.9, their convergent rates of the output voltage errors will be slower than those with larger λ.

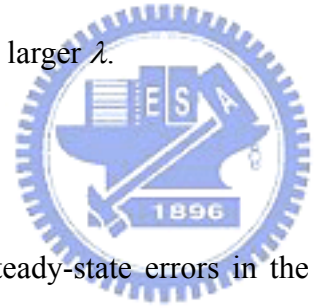

Remark 3.1

From Fig. 3.9, there are steady-state errors in the output voltages, which can be reduced if λ is increased. The steady-state errors result from the use of phase-variable control canonical form in the design of sliding function, which is equivalent to a PD-type feedback control [19,45]. Another reason of the existence of steady-state errors is that the averaging value of the sliding function may not be ideally zero [26].

Example 3.2:

Let λ=100, 3500 and 20000. The experimental results are shown in Fig. 3.10, Fig. 3.11 and Fig. 3.12. Fig. 3.10 shows three system trajectories with λ=100, 3500 and 20000. The system trajectory with λ=100 has been described in example 3.1. As for the system trajectories with λ=3500 and 20000, they correspond to the cases of Type-II that goes through J_2 and J_4 respectively. Note that there exists DCM during the

transient state in the case with λ=20000. From Fig. 3.11, it can also be found that the sliding functions with λ=3500 and λ=20000 do not always converge since the RAS-condition for the cases of Type-II is not globally satisfied. However, these system trajectories will eventually enter the RAS-region and reach the sliding line after a short time. Unlike example 3.1, Fig. 3.12 shows that larger λ will lead to larger overshoot, which may not be desired in some applications.

In this example, it shows that the experimental results actually confirm the switching behaviors described in §3.3 and the bang-bang sliding mode control can successfully drive these system trajectories into the corresponding sliding lines.

Example 3.3:

Let λ=1000, 3300 and 4000 and connect the buck DC-DC converter to a variable resistive load with the value of 20.5Ω and 6.9Ω. Fig. 3.13 shows the output voltage errors of experimental results, where the sub-figures on the left side demonstrate the transient state from light load (3W) to heavy load (9W) and the sub-figures on the right side demonstrate the transient state from heavy load to light load. Obviously, if λ is chosen to be larger than 1000, the buck DC-DC converter will possess the robustness to load variations with less than 0.3V deviation, *i.e.*, less than 3.75% of V_d.

■

From above examples, we can choose a suitable λ to attain the desired performances, as summarized in Table 3.3. If the overshoot is larger than the desired specification, it can be improved by decreasing the value of λ according to Fig. 3.12. If the steady-state error of the output voltage is larger than the acceptable value, it can be reduced by increasing λ according to Fig. 3.9. While the convergent rate is too slow, it can be accelerated by increasing λ also viewing from Fig. 3.9.

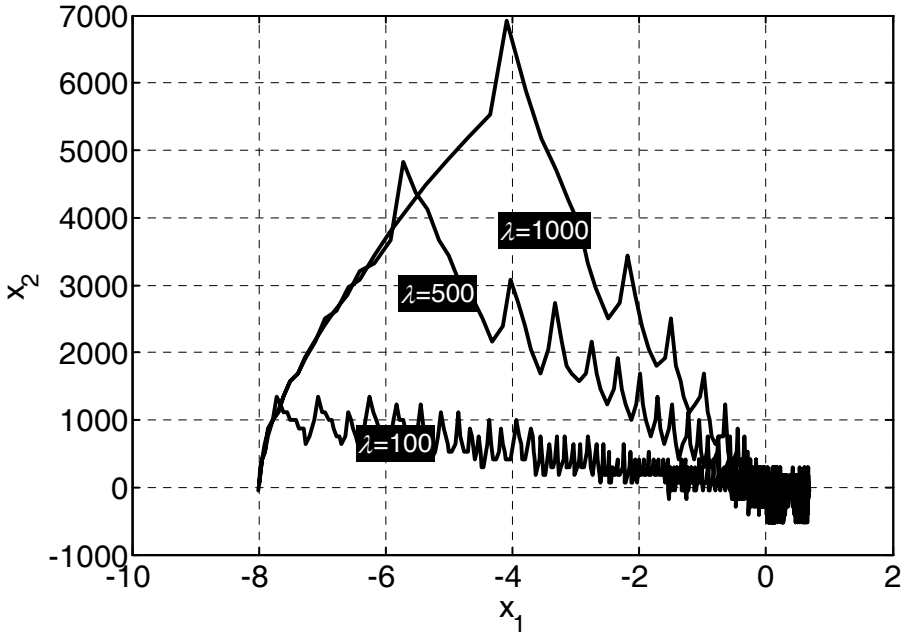

Fig. 3.7 System trajectories with different λ in example 3.1.

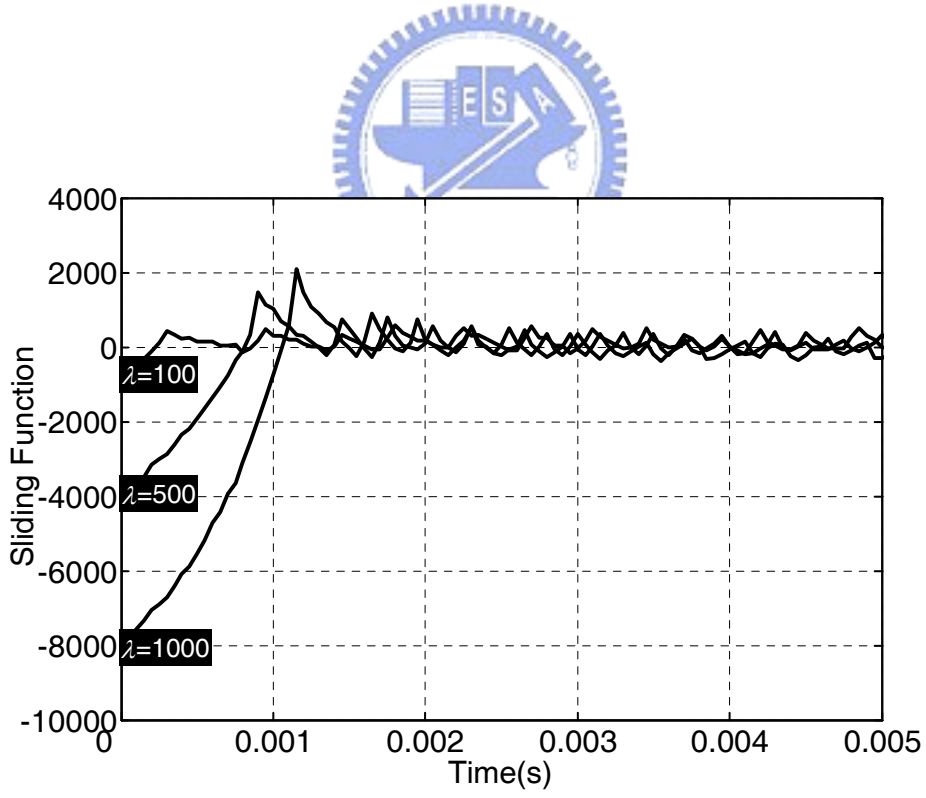

Fig. 3.8 Sliding functions with different λ in example 3.1.

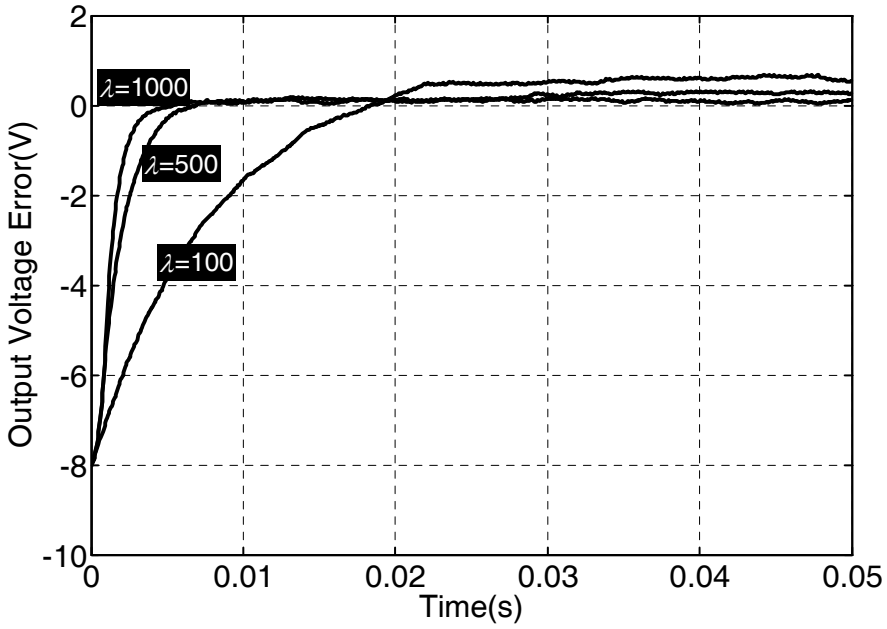

Fig. 3.9 Output voltage errors with different λ in example 3.1.

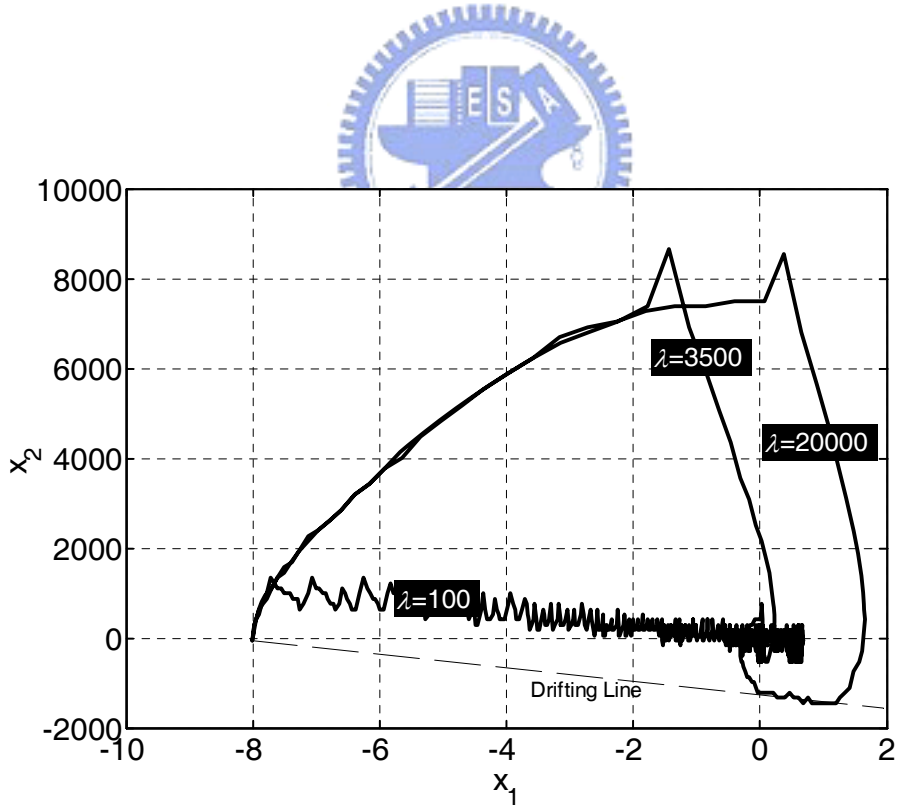

Fig. 3.10 System trajectories with different λ in example 3.2.

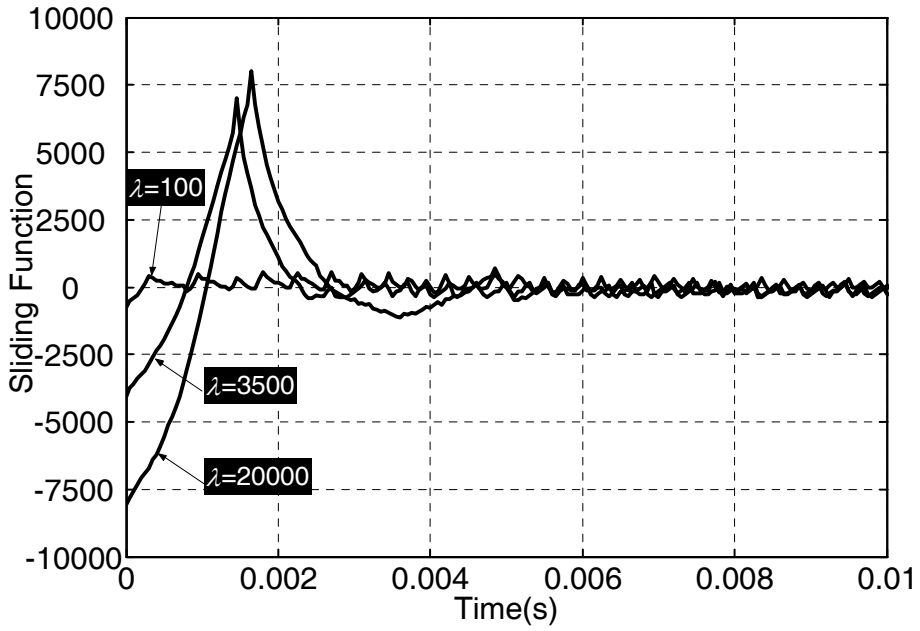

Fig. 3.11 Sliding functions with different λ in example 3.2.

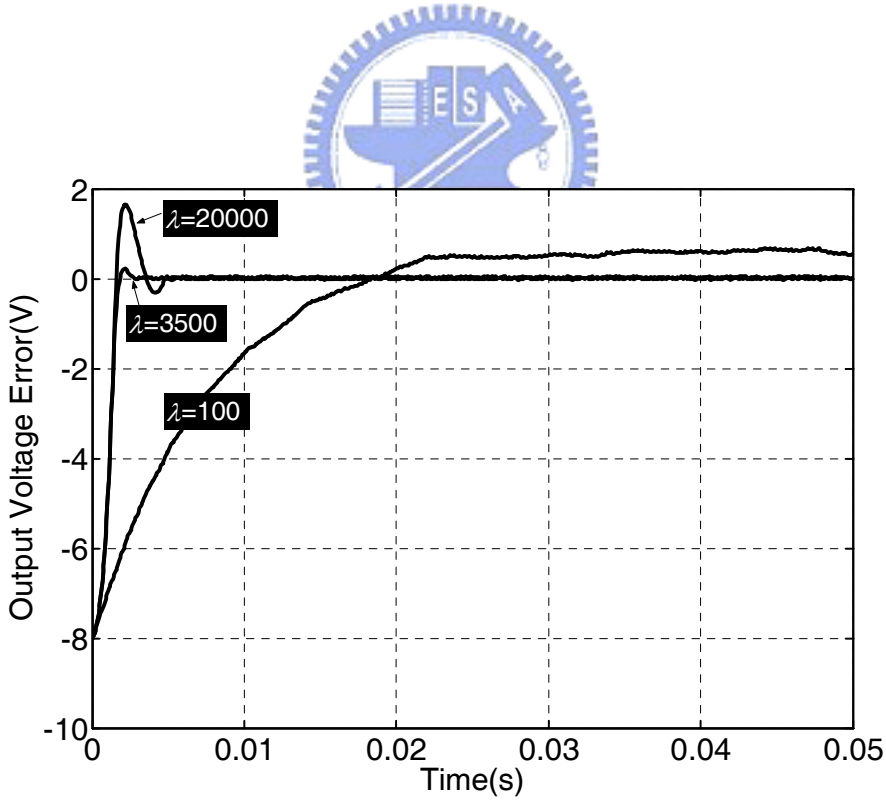

Fig. 3.12 Output voltage errors with different λ in example 3.2.

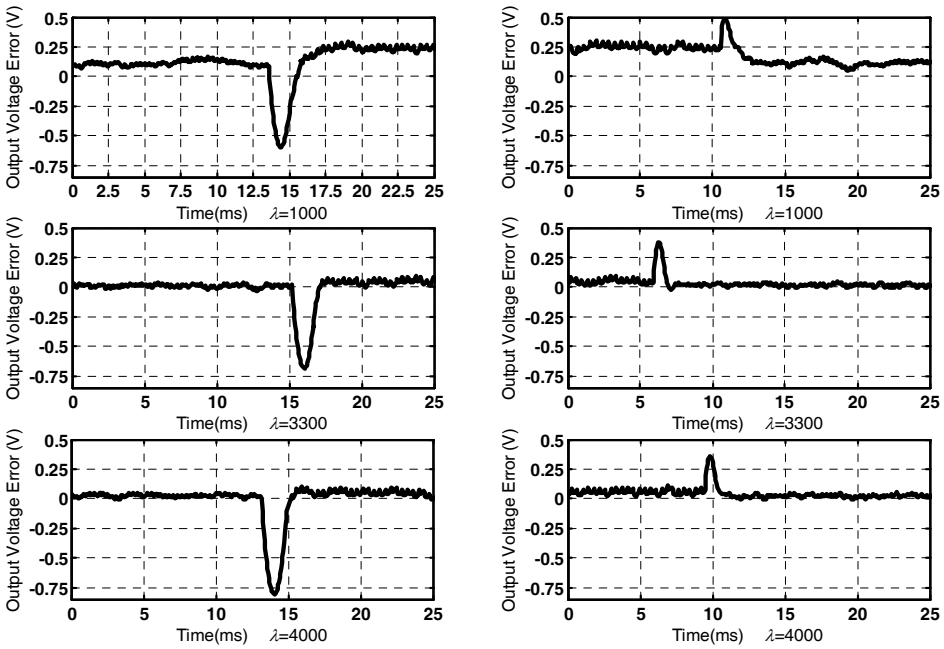

Fig. 3.13 Output voltage errors by load variations.

Table 3.3 Tune-up of λ in terms of the desired performance.

Desired performance	λ
Reduce overshoot	Decreased
Reduce output error	Increased
Increase convergent rate	Increased

3.4 Discussions

Theoretical analyses of the bang-bang sliding mode control for a buck DC-DC converter are given in §3.2, and the hardware to realize the control algorithm in the PC-based environment is demonstrated in §3.3. It shows that the experimental results agree with the theoretical analyses. However, there are still some gaps between the PC-based controller and the practical controller by analog circuits such that the original control algorithm could not be directly implemented. Thus, some modifications for practical design will be included in this section. Besides, there exists unavoidable switching frequency deviation in the bang-bang sliding mode controller, which results from different sliding functions, input voltage, output voltage and load variations. The deviation in switching frequency is not desired since it makes the input and output filters design more difficult. Based on the method proposed in [25], a periodic ramp signal will be adopted in this section to achieve the constant switching frequency. More detailed discussions about the bang-bang sliding motions in the steady state will be given. Finally, numerical simulations will demonstrate the effectiveness by these modifications and some conclusions will be given.

3.4.1 Modifications of State Variables and Sliding Function

Usually, there is only one external reference voltage V_{ref} available in analog circuits. The sensed output voltage v_o cannot be directly compared with V_{ref} but should be scaled with a predetermined scalar α. Therefore, the original state variable x_1 will be redefined by a new variable z_1 as

$$z_1 = \alpha v_o - V_{ref} = \alpha\left(v_o - \frac{V_{ref}}{\alpha}\right) = \alpha\left(v_o - V_d\right) = \alpha x_1 \tag{3.30}$$

Obviously, α is determined from the ratio of V_{ref} to V_d and z_1 is x_1 multiplied by α. Similar to the procedures in §3.1, define another state variable z_2 as the derivative of z_1 with respective to time, *i.e.*,

$$z_2 = \frac{dz_1}{dt} = \alpha \frac{dx_1}{dt} = \alpha x_2 \tag{3.31}$$

From (3.30) and (3.31), the system dynamics is represented as

$$\dot{\boldsymbol{z}} = \begin{bmatrix} 0 & 1 \\ -\dfrac{1}{LC} & -\dfrac{1}{RC} \end{bmatrix} \boldsymbol{z} + \begin{bmatrix} 0 \\ \dfrac{\alpha E}{LC} \end{bmatrix} u + \begin{bmatrix} 0 \\ -\dfrac{V_{ref}}{LC} \end{bmatrix} \tag{3.32}$$

where $\boldsymbol{z}$ is $[z_1 \ z_2]^T$. Note that r_d is neglected in this section for simplification. Compared with (3.5), z_1 and z_2 are the original state variables multiplied by α, the input vector is $\boldsymbol{B}$ multiplied by α and the external input vector is $\boldsymbol{h}$ scaled down by α. The system matrix $\boldsymbol{A}$ is unchanged and thus the system dynamics of (3.32) is still the same as (3.5). As for the RAS-region, it can also be derived from the similar procedures described in §3.2.

With the state variables z_1 and z_2, the sliding function becomes

$$s = z_2 + \lambda z_1 = \alpha\left(x_2 + \lambda x_1\right) \tag{3.33}$$

Note that, in (3.25), to make RAS-region large enough, λ is usually chosen as β/C, where β=1/R and R is supposed to be known. Then, substituting the feedback signals into (3.33), it results in

$$s = \frac{\alpha}{C} i_C + \frac{\alpha\beta}{C}\left(v_o - V_d\right) \tag{3.34}$$

In switching power converters, the value of capacitance C is typically in the range of microfarad. Therefore, the coefficients in (3.34) will be too large for practical implementation, *e.g.*, in analog circuits, saturations may occur in operational amplifiers. A straightforward idea to solve this problem is multiplying the sliding function with a scalar γC. Then, the sliding function eventually becomes

$$s = \gamma C\left(z_2 + \lambda z_1\right) = \gamma\left(\alpha i_C + \beta\left(\alpha v_o - V_{ref}\right)\right) \tag{3.35}$$

where γ is an adjustable positive number. Note that multiplying the sliding function with γC will not affect the overall system dynamics and the RAS-region, and it makes the sliding function independent of capacitance value. Now, there are two undetermined parameters β and γ in (3.35). For β, it is equivalent to λ and can be adjusted according to Table 3.3. As for γ, it is used to scale the original sliding function in a reasonable range.

3.4.2 Constant Switching Frequency Strategy

Practically, the switching power converters cannot operate at an infinite switching frequency and a hysteresis band is usually used by the SMC-based controllers. However, the switching frequency of the hysteresis-type SMC-based controller is affected by line and load variations and thus, several methods as introduced in Chapter 1 have been proposed to modify the SMC-based controllers to control switching power converters at a constant switching frequency.

In order to achieve the same purpose, the bang-bang sliding motions inside the hysteresis region will first be discussed. Then, a brief review of existing methods for SMC-based controllers will be given. Finally, the simplest method of adding a periodic ramp signal to control bang-bang sliding motions at a constant frequency will be discussed.

A) Bang-Bang Sliding Motions Inside the Hysteresis Region

In the sliding mode theory, the input is assumed to be capable of switching at an infinite frequency such that the controlled system can be theoretically in the sliding mode. However, for the switching power converters, the switching devices cannot be operated with an infinite switching frequency and thus a hysteresis band is usually

introduced to avoid this unachievable requirement. While a hysteresis band is introduced around the s=0, the control law in (3.11) will become

$$u = \begin{cases} 0, & s > \varepsilon \\ 1, & s < -\varepsilon \end{cases} \tag{3.36}$$

where ε is the width of the hysteresis band. In the steady-state operation, the bang-bang sliding motions inside the hysteresis region are illustrated in Fig. 3.14, in which $f(\mathbf{z},u^-)$ and $f(\mathbf{z},u^+)$ denote the vectors of state variable velocity with u^-=1 and u^+=0 respectively. The time taken for $f(\mathbf{z},u^-)$ to move from point P to point Q and the time taken for $f(\mathbf{z},u^-)$ to move from point Q to point R are denoted as Δt_1 and Δt_2, which can be calculated by

$$\begin{aligned} \Delta t_1 &= \frac{2\varepsilon}{grad(s)\cdot f(\mathbf{z},u^-)} \\ \Delta t_2 &= \frac{-2\varepsilon}{grad(s)\cdot f(\mathbf{z},u^+)} \end{aligned} \tag{3.37}$$

As shown in [19], if λ is ideally chosen as $1/RC$, the switching frequency f_{sw} can be approximately obtained as

$$f_{sw} = \frac{1}{T} = \frac{1}{\Delta t_1 + \Delta t_2} = \frac{v_C\left(1-\frac{v_C}{E}\right)}{2\varepsilon L} \tag{3.38}$$

From (3.38), f_{sw} is mainly affected by the variations of input voltage and output voltage. Besides, if the resistive load is not exactly known (*i.e.*, λ cannot be exactly set as $1/RC$), it will also affect f_{sw}. With the hysteresis band being used, the control scheme of the hysteresis-type bang-bang sliding mode controller is shown in Fig. 3.15.

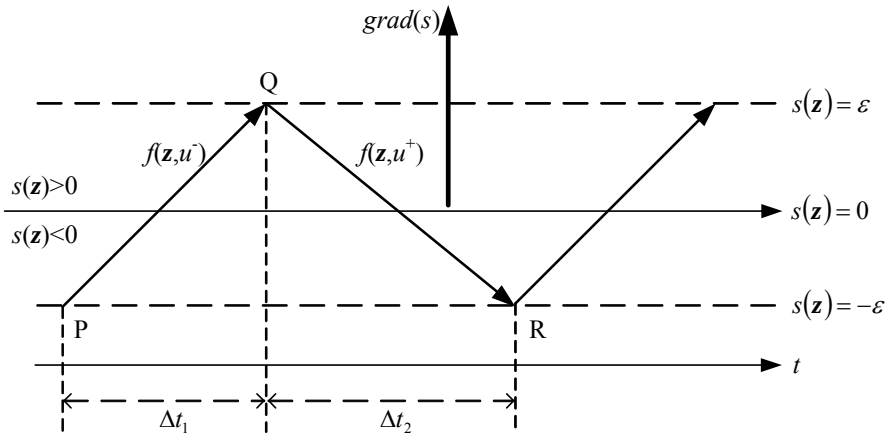

Fig. 3.14 Bang-bang sliding motions inside the hysteresis region.

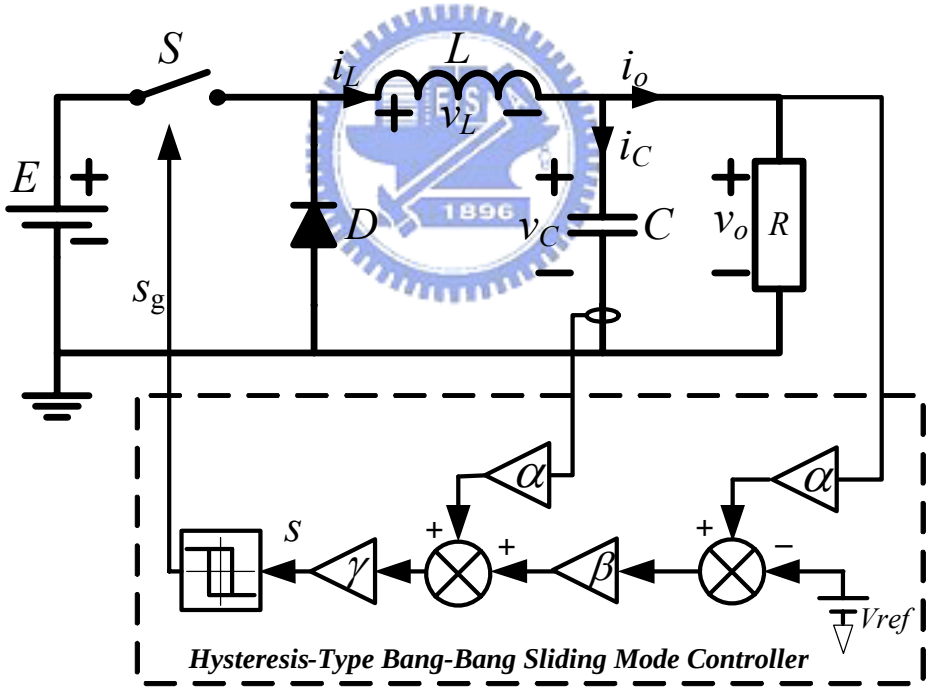

Fig. 3.15 Hysteresis-type bang-bang sliding mode controller

B) Existing methods for fixed frequency sliding mode controller

As discussed in previous paragraph, f_{sw} is highly dependent on the input voltage, output voltage and the resistive load. To control the switching power converters at a constant f_{sw}, several methods have been briefly introduced in Chapter 1. In [20], an extra state defined as the integral of output voltage error is used to formulate the specific sliding function, which results in a PID-type PWM controller. Then, the equivalent control u_{eq} can be derived from the invariance conditions in the sliding mode. However, R is still involved in the representation of u_{eq} such that u_{eq} cannot be perfectly realized. Compared with [20], the sliding function in [24] is designed as the function of inductor current, output voltage and the integral of output voltage error. With this sliding function, the system is initially in the sliding mode, *i.e.*, $s(t=0)=0$. As a result, u_{eq} can be theoretically obtained for all time. Significantly, an adaptive law is proposed to eliminate the effect of the un-modeled parasitic resistance in the circuit. In [21], the idea of adopting a variable hysteresis band adjusted by adaptive feedforward and feedback control is proposed. The adaptive feedforward loop is used to reduce the deviation of f_{sw} resulting from the input voltage variation. As for the adaptive feedback loop, it is used to adjust the coefficients of the sliding function such that the deviation of f_{sw} resulting from the load variation can also be reduced. Actually, the measuring of input voltage is needed for the adaptive feedforward control scheme to directly change the width of hysteresis band ε, and the measuring of the output load current i_o is also needed for the adaptive feedback control scheme to compute the resistive load R. The simplest method is that proposed in [26], which is implemented by adding a periodic ramp signal and a PI-type compensator into the hysteresis-type sliding mode controller. This method possesses the advantages that f_{sw} is constant under all operation conditions and it can be directly controlled by varying the frequency of the periodic ramp signal. Therefore, it will be used in this dissertation

and some design considerations will be given in the next.

C) Hysteresis-Type Bang-Bang Sliding Mode Controller at fixed-frequency

First, define a periodic ramp signal s_{ramp} with the amplitude, frequency and period being denoted as $\varepsilon_{\text{ramp}}$, f_{ramp} and T_{ramp} respectively. Then, add s_{ramp} into the original control scheme as the block diagram shown in Fig. 3.16, in which s_{c} is the summation of s and s_{ramp}, s_{g} is the gate driver signal and ε_s is the hysteresis band of s. The ideal steady-state waveforms of s, s_{ramp} and s_{c} are given Fig. 3.17. From Fig. 3.17, it can be found that these signals should satisfy the following equations:

$$\left(s\big|_{t=0} + \int_0^{\Delta t_{\text{on}}} \dot{s}\big|_{u=1}\, dt \right) + \left(-\varepsilon_{\text{ramp}} + \frac{2\varepsilon_{\text{ramp}}}{T_{\text{ramp}}} \Delta t_{\text{on}} \right) = s_{\text{c}}\big|_{t=\Delta t_{\text{on}}} = \varepsilon \tag{3.39}$$

and

$$\left(s\big|_{t=\Delta t_{\text{on}}} + \int_{\Delta t_{\text{on}}}^{T_{\text{ramp}}} \dot{s}\big|_{u=0}\, dt \right) + \left(-\varepsilon_{\text{ramp}} \right) = s_{\text{c}}\big|_{t=T_{\text{ramp}}} < -\varepsilon \tag{3.40}$$

Note that (3.39) and (3.40) are used to guarantee that S will switch off during each cycle and it can immediately switch on at the beginning of each cycle. To satisfy (3.40), $\varepsilon_{\text{ramp}}$ is typically chosen to be larger than ε.

While a converter operates at a constant switching frequency, $\Delta t_{\text{on}}/T_{\text{ramp}}$ is equivalent to the duty cycle d and (3.39) can be expressed as

$$\varepsilon_s + (2d-1)\varepsilon_{\text{ramp}} = \varepsilon \tag{3.41}$$

Besides, (3.40) can be rewritten

$$-\varepsilon_s - \varepsilon_{\text{ramp}} < -\varepsilon \tag{3.42}$$

Obviously, when f_{sw} is synchronizing to f_{ramp}, the bang-bang sliding motions inside the hysteresis region will be governed by (3.41) and (3.42). From (3.41), if the averaging value of s is zero, ε_s will be smaller than ε when d>0.5, and ε_s will be larger than ε when d<0.5. The waveforms with d>0.5 have been shown in Fig. 3.17 and the waveforms with d<0.5 are given in Fig. 3.18 as a comparison.

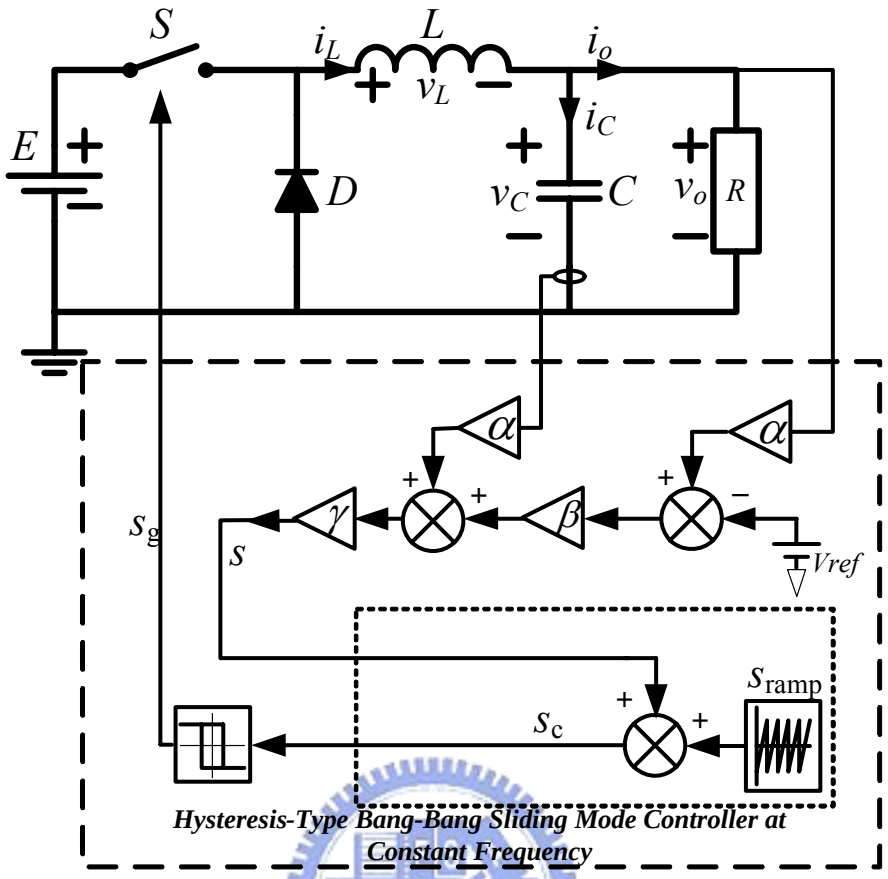

Fig. 3.16 Hysteresis-type bang-bang sliding mode controller at switching constant frequency.

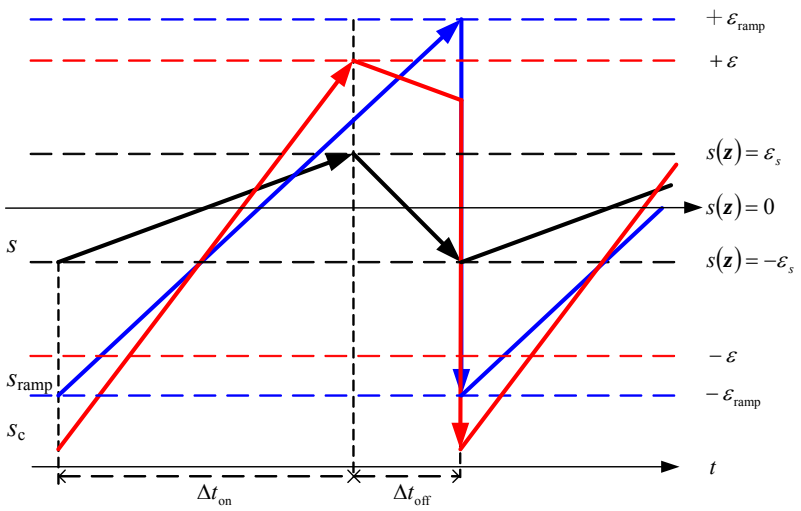

Fig. 3.17 Waveforms of the signals inside the hysteresis region (d>0.5).

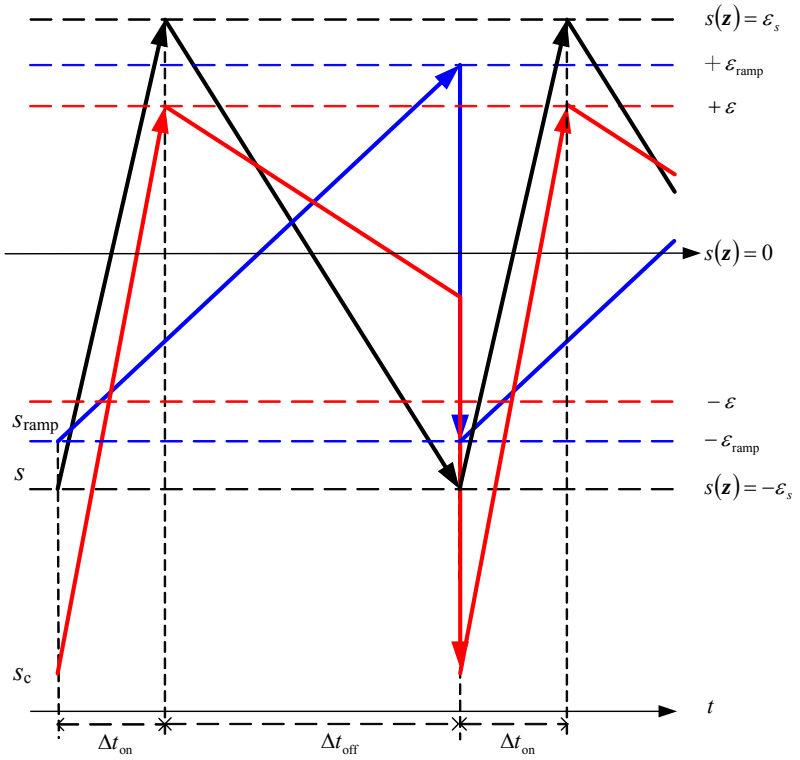

Fig. 3.18 Waveforms of the signals inside the hysteresis region (d<0.5).

Ideally, s_{ramp} should not affect the averaging value of s. But, it may deteriorate s such that the averaging value of s will be a nonzero value ε_0. In this situation, the waveforms are non-ideal as given in Fig. 3.19, where ε_0=0.5(ε_{s1}−ε_{s2}), and ε_{s1} and ε_{s2} are not necessary to be positive. The equations of (3.41) and (3.42) will become

$$\varepsilon_{s1}+(2d-1)\varepsilon_{\text{ramp}}=\varepsilon \tag{3.43}$$

and

$$-\varepsilon_{s2}-\varepsilon_{\text{ramp}}<-\varepsilon \tag{3.44}$$

The waveforms with positive ε_0 have been shown in Fig. 3.19 and the waveforms with negative ε_0 are also given in Fig. 3.20 as a comparison. Compared with Fig. 3.18, d is smaller when ε_0 is positive, and d is larger when ε_0 is negative. Thus, a nonzero ε_0 may lead to steady-state error in the output voltage. In order to reduce the steady-state error, a PI-type compensator will be further incorporated into the control scheme and the block diagram is shown in Fig. 3.21.

In next section, numerical simulations based on the control scheme in Fig. 3.16 will

first be given to show the effectiveness of adding an additional periodic ramp signal for achieving constant switching frequency. Then, a PI-type compensator will further be incorporated into the controller and numerical simulations will demonstrate the reduction of the steady-state error in the output voltage.

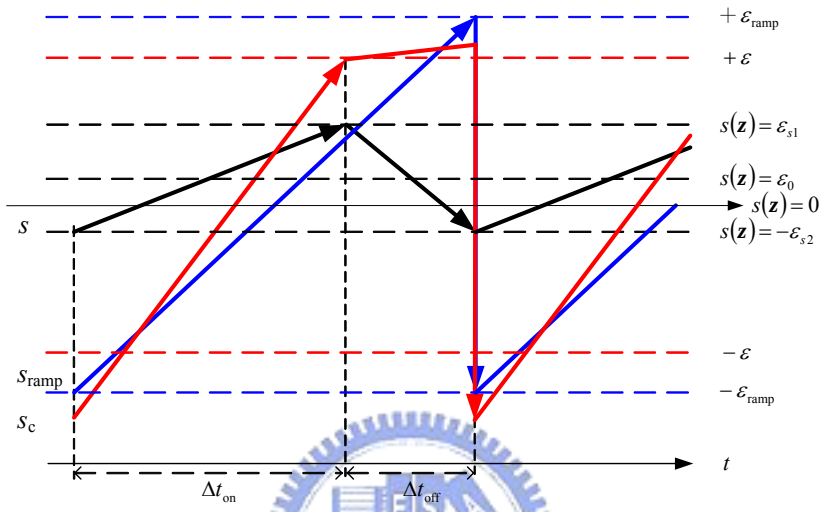

Fig. 3.19 Waveforms of the signals inside the hysteresis region (ε_0 >0).

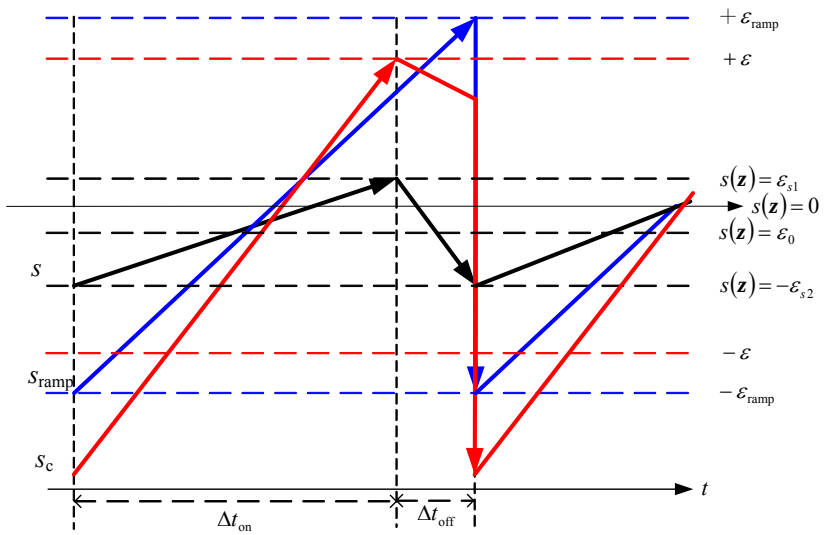

Fig. 3.20 Waveforms of the signals inside the hysteresis region (ε_0 <0).

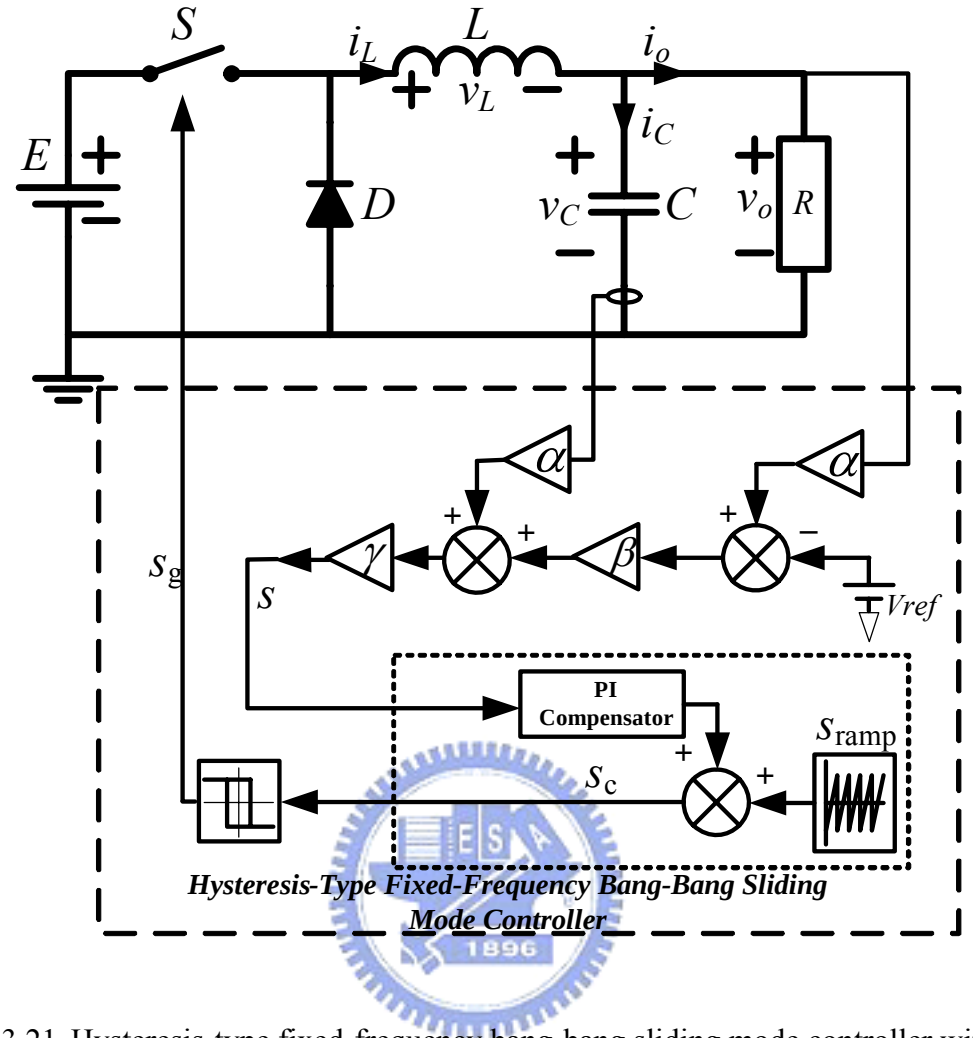

Fig. 3.21 Hysteresis-type fixed-frequency bang-bang sliding mode controller with a PI-type compensator.

3.4.3 Numerical Simulation Results

Consider a buck DC-DC converter with the same parameters listed in Table 3.2 and set ε as 0.1. The parameters β and γ of the sliding function in (3.35) are chosen as 0.5 and 1. In the following examples, it will first show the simulation results with only the periodic ramp signal s_{ramp} being added, as the control scheme in Fig. 3.16. Then, the bang-bang sliding motions inside the hysteresis region with different V_d and different ε_{ramp} will be discussed. Finally, the control scheme in Fig. 3.21 will be employed to shown the effectiveness of reducing steady-state errors by incorporating the PI-type

compensator.

Example 3.4

Consider four cases with the desired output voltage V_d being set as (a) 3V, (b) 5V, (c) 7V and (d) 10V. When the reference voltage V_{ref} is provided as 3.3V, the corresponding α are calculated as the values of 1.1, 0.66, 0.47 and 0.33. Besides, f_{ramp} is set as 20kHz and $\varepsilon_{\text{ramp}}$ is set as 0.5. The simulation results of the output voltage errors by percentage in four cases are presented in Fig. 3.22 and the system trajectories are shown in Fig. 3.23, in which the x-axis and y-axis are defined in the output voltage and capacitor current. Viewing from Fig. 3.22, there exist un-avoidable steady-state errors in the output voltage and the minimum error will occur in the situation when V_d is about half of input voltage, *i.e.*, d is around 0.5. For the case (a) and case (d), the steady-state errors even exceed 10%. The waveforms of case (b) and case (d) are represented in Fig. 3.24 and Fig. 3.25. Obviously, ε_0 is positive in Fig. 3.24 and negative in Fig. 3.25, which correspond to the situations in Fig. 3.19 and Fig. 3.20 respectively. Besides, the gate signal s_g will synchronize to s_{ramp} if $\varepsilon_{\text{ramp}}$ is properly chosen to be enough larger than ε. In this example, $\varepsilon_{\text{ramp}}$ is 5 times the value of ε.

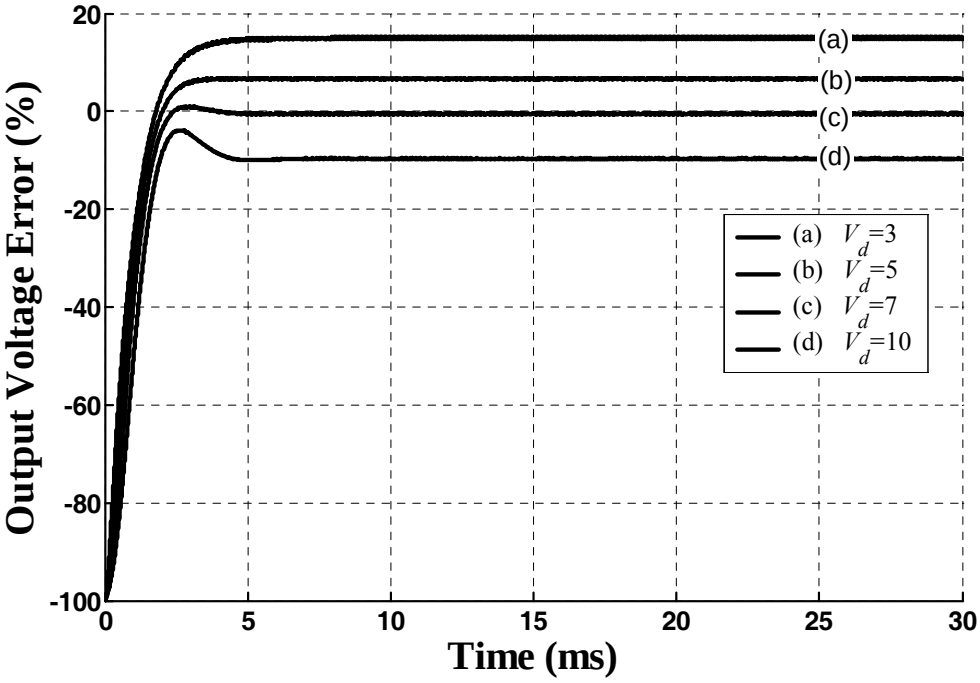

Fig. 3.22 Output voltage errors by percentage in four cases with different V_d.

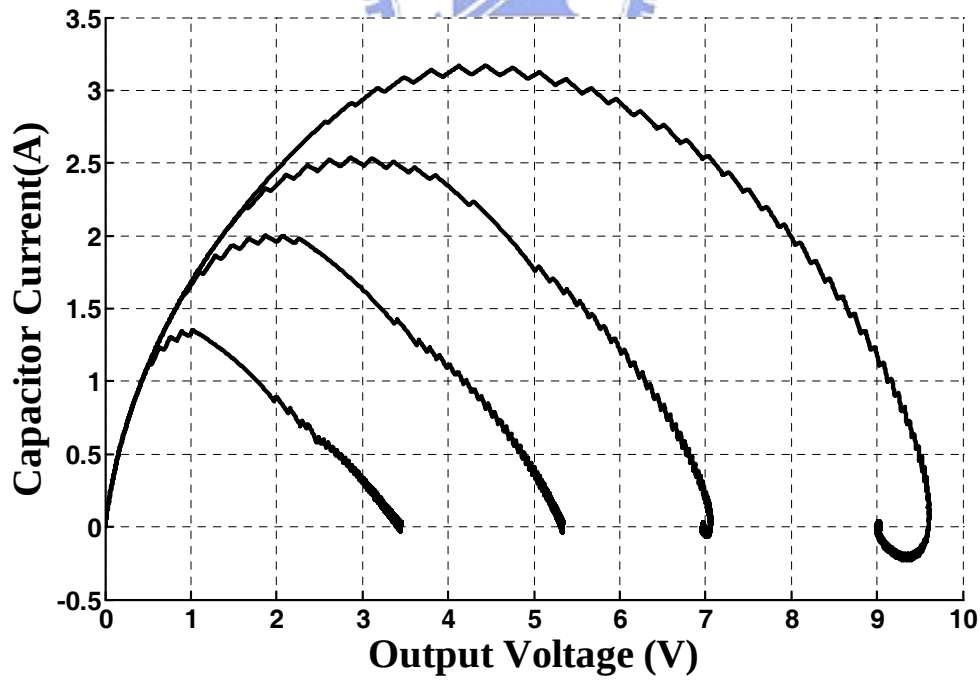

Fig. 3.23 System trajectories in four cases with different V_d.

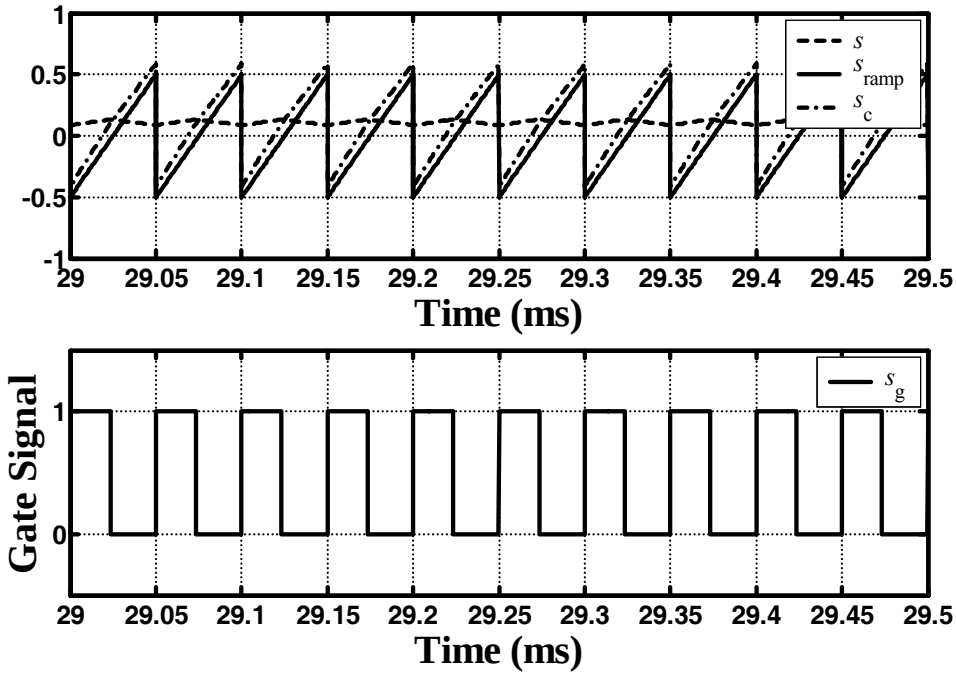

Fig. 3.24 Waveforms of the case with V_d=5V.

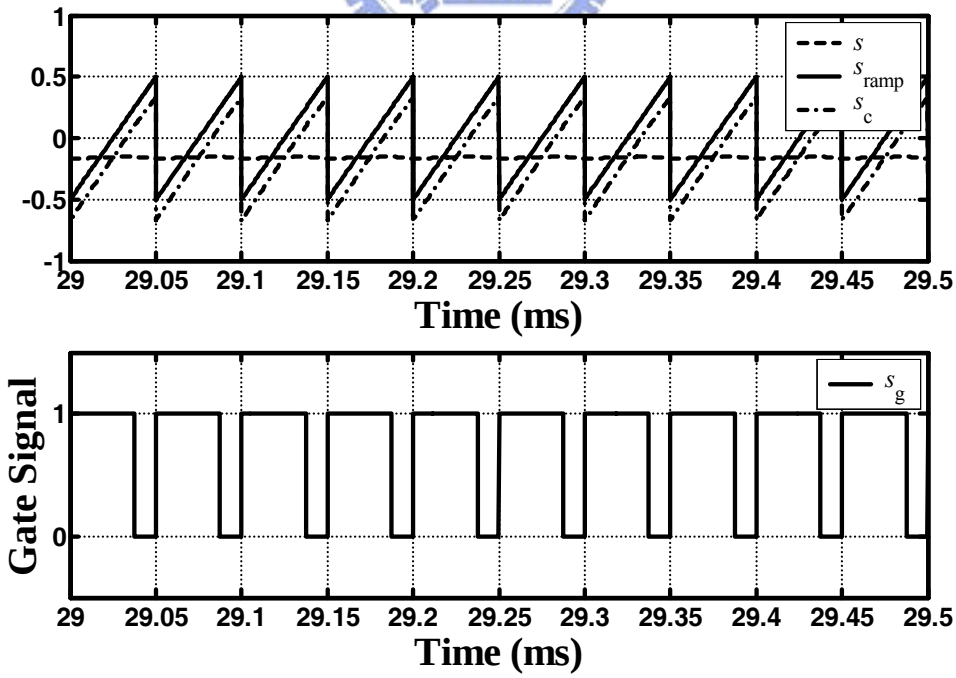

Fig. 3.25 Waveforms of the case with V_d=10V.

Example 3.5

Consider four cases with ε_{ramp} being set as (a) 0.15, (b) 0.25, (c) 1 and (d) 5. Let V_d be 5V and then α is calculated as 0.66 for these cases. The simulation results of the output voltage errors by percentage in four cases are presented in Fig. 3.26. From Fig. 3.26, with the same V_d, the steady-state error will be increased when ε_{ramp} is increased. It results from that ε_0 is larger for the cases with larger ε_{ramp}, as shown in Fig. 3.27. Although the best output performance exists in case (a), s_g will not synchronize to s_{ramp} and the waveforms of this case are represented in Fig. 3.28. In this example, it shows that ε_{ramp} should be chosen larger enough to guarantee that s_g can synchronize to s_{ramp}. However, larger ε_{ramp} may make the steady-state error beyond the acceptable range. In next example, a PI-type compensator will be incorporated into the control scheme to reduce the steady-state errors.

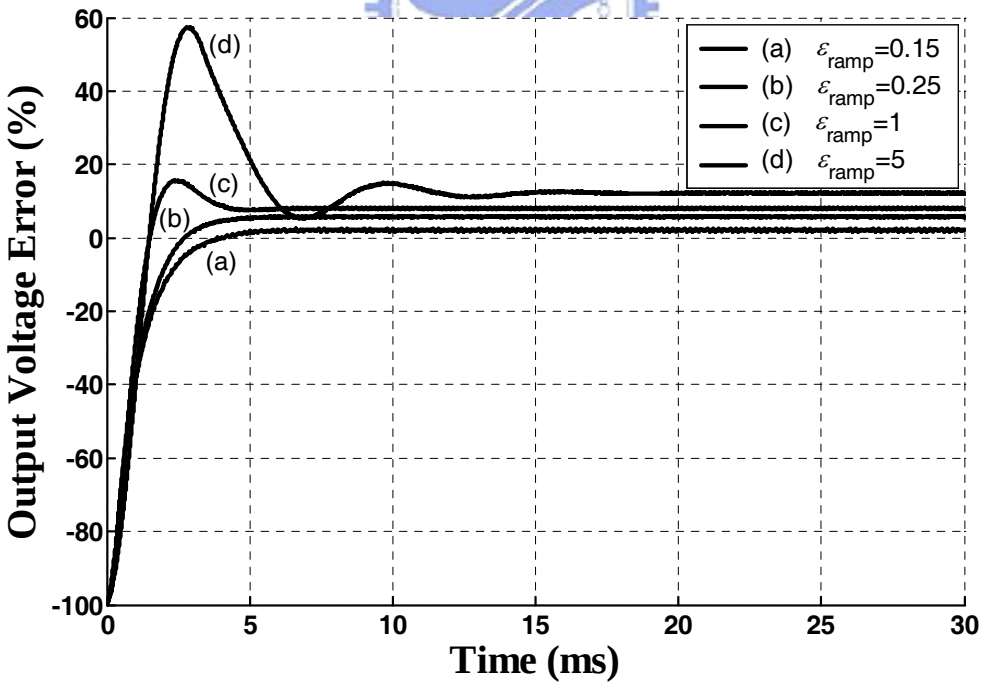

Fig. 3.26 Output voltage errors by percentage in four cases with different ε_{ramp}.

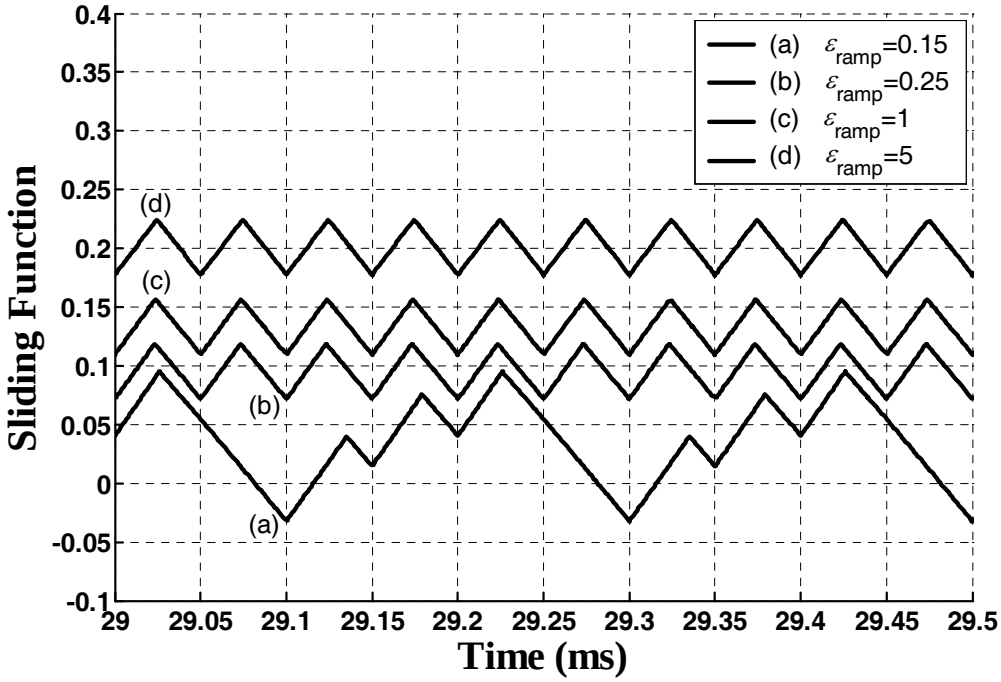

Fig. 3.27 Steady states of sliding functions in four cases with different ε_{ramp}.

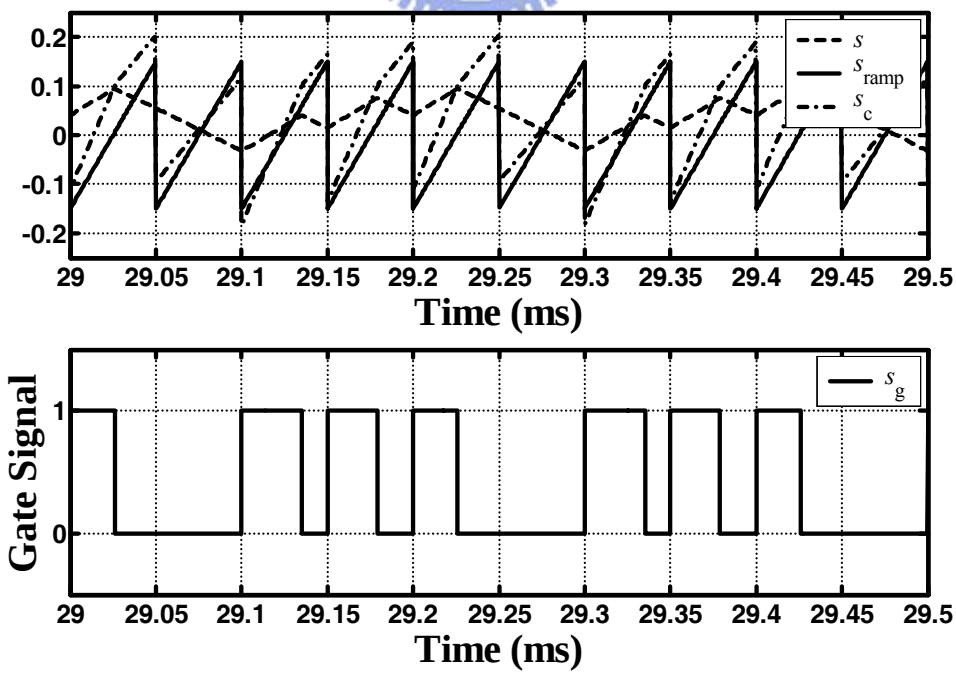

Fig. 3.28 Waveforms of the case (d) in example 3.5.

Example 3.6

Let ε_{ramp}=1 and V_d=5 and introduce a PI-type compensator into the control scheme as shown in Fig. 3.21, where the proportional constant and integral constant are defined as K_P and K_I. Then, consider three cases with K_P being set as the same value of 1 and K_I being set as (a) 50, (b) 100 and (c) 200 respectively. To show the effectiveness of adding a PI-type compensator, the simulation results are represented in Fig. 3.29. Obviously, the steady-state errors can be effectively eliminated and the buck DC-DC converter can operate at a desired frequency f_{ramp} by the modified bang-bang sliding mode control scheme given in Fig. 3.21. The waveforms of case (c) are given in Fig. 3.30, in which s_{ramp} and s_c are scaled down and the magnitude of s is too small such that s_{ramp} and s_c are almost the same. Note that there will exist a very small deviation in s for compensating the steady-state error.

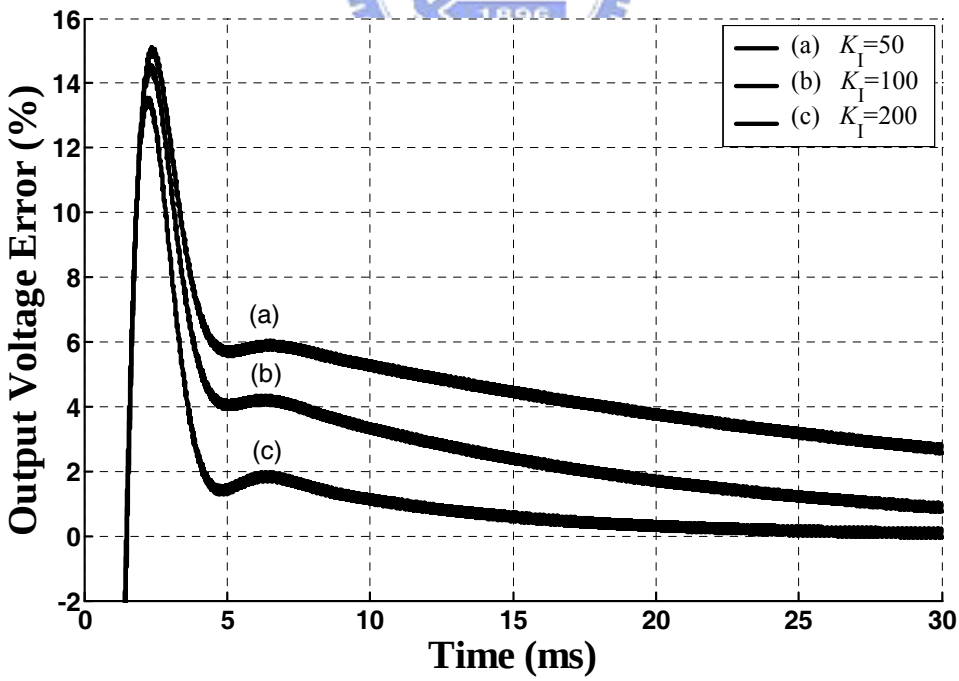

Fig. 3.29 Output voltage errors by percentage in three cases with different K_I.

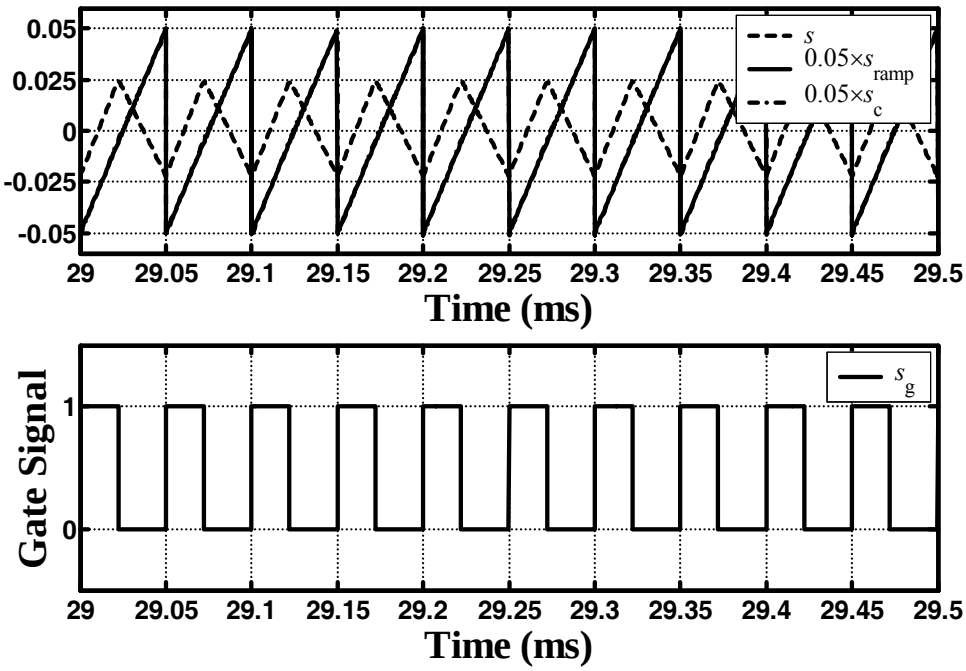

Fig. 3.30 Waveforms of the case (c) in example 3.6.

Some considerations for practical implementation by analog circuits are first given in §3.4.1. Then, the original controller is modified to operate at a constant switching frequency in §3.4.2 and the steady-state bang-bang sliding motions inside the hysteresis region are clearly discussed. In §3.4.3, the simulation results are given to demonstrate the effectiveness of the proposed control scheme. Altogether, the purposes of scaling the original sliding function into a reasonable range and controlling the buck DC-DC converter at a constant switching frequency are both achieved.

Chapter 4 Bang-Bang Sliding Mode Control in Switched Systems

In this chapter, a switching controller based on the bang-bang sliding mode control will be proposed for a class of switched systems consisting of two second-order unstable subsystems. In §4.1, the stabilization problem in these switched systems is first briefly introduced and two important assumptions will be given for the bang-bang sliding mode control to guarantee the existence of stable sliding motions. Then, the design procedures and the system stabilities related to three types of reaching modes are provided in §4.2. Another class of switched systems with model uncertainties is considered in §4.3 and the robustness of the bang-bang sliding mode control to model uncertainties will be discussed. Finally, several numerical simulation results are demonstrated in §4.4.

4.1 Problem Statement

Consider a switched system consisting of two second-order subsystems, given by

$$\dot{\boldsymbol{x}} = \boldsymbol{A}_{\sigma(t)}\boldsymbol{x} \tag{4.1}$$

where $\sigma(t):[0,\infty)\to\{1,2\}$, $\boldsymbol{x}\in\boldsymbol{R}^2$ and both $\boldsymbol{A}_1$ and $\boldsymbol{A}_2$ are 2×2 constant non-Hurwitz matrices. The main purpose in this chapter is to determine the switching conditions for these two subsystems such that the overall system dynamics is stabilized.

Interestingly, (4.1) can be rewritten into a second-order homogeneous bilinear system, similar to the procedure in [37], controlled by a switching input as

$$\dot{\boldsymbol{x}} = \boldsymbol{A}\boldsymbol{x} + u\boldsymbol{N}\boldsymbol{x} \tag{4.2}$$

where $\boldsymbol{A}$=0.5($\boldsymbol{A}_1$+$\boldsymbol{A}_2$), $\boldsymbol{N}$=0.5($\boldsymbol{A}_1$−$\boldsymbol{A}_2$) and the switching input $u\in\{-1, 1\}$. Clearly, the stabilization problem in (4.1) is equivalent to designing the switching input u to stabilize (4.2). To deal with the stabilization problem in (4.2), first define λ_i and $\boldsymbol{c}_i$ as the i-th eigenvaule and its corresponding left eigenvector of $\boldsymbol{A}+u_0\boldsymbol{N}$, where u_0 is a real number. Then, the bang-bang sliding mode control is proposed to stabilize the system (4.2) under the following assumptions:

Assumption 4.1.

There exists a u_0 *in the range of* (−1, 1) *such that the eigenvalues,* λ_1 *and* λ_2, of $\boldsymbol{A}+u_0\boldsymbol{N}$ *are stable and real*.

Assumption 4.2.

There exists at least one left eigenvector $\boldsymbol{c}_i$ *corresponding to* λ_i *that satisfies* *rank*($[\boldsymbol{c}_i;\boldsymbol{c}_i\boldsymbol{N}]$)=2.

Similar to several literatures [32-34], the existence of stable matrices combination $\boldsymbol{A}+u_0\boldsymbol{N}$ is also required in this dissertation. Besides, λ_1 and λ_2 are further assumed to be real, as declared in Assumption 4.1, such that their left eigenvectors $\boldsymbol{c}_1$ and $\boldsymbol{c}_2$ are real and could be used as the coefficient vector of a sliding function [13,46]. As for Assumption 4.2, it is required to guarantee the existence of stable sliding motions, which will be explained later.

In next section, with both assumptions being satisfied, a switching controller based on the bang-bang sliding mode control will be proposed for the homogenous bilinear system (4.2). It will show that the switching input must be determined from two switching functions rather than a single one as the general sliding controls. The stability of the switched system will be proven and different switching behaviors resulting from these two switching functions will be clearly described.

4.2 Design Procedures of Bang-Bang Sliding Mode Control

Under Assumption 4.1, system (4.2) can be further rewritten as

$$\dot{\boldsymbol{x}} = \boldsymbol{A}_{\mathrm{S}}\boldsymbol{x} + u_{\mathrm{S}}\boldsymbol{N}\boldsymbol{x} \tag{4.3}$$

where $\boldsymbol{A}_{\mathrm{S}}=\boldsymbol{A}+u_0\boldsymbol{N}$, $u_{\mathrm{S}}=-u_0+u$ and $u\in\{-1, 1\}$. Obviously, system (4.3) is still a homogeneous bilinear system but possesses a stable system matrix $\boldsymbol{A}_{\mathrm{S}}$ with real eigenvalues and a new input u_{S}. Let λ be one of the eigenvalues of $\boldsymbol{A}_{\mathrm{S}}$ and $\boldsymbol{c}$ be the corresponding left eigenvectors, *i.e.*,

$$\boldsymbol{c}\boldsymbol{A}_{\mathrm{S}} = \lambda\,\boldsymbol{c} \tag{4.4}$$

Then, the sliding function $s(\boldsymbol{x})$ can be defined as

$$s(\boldsymbol{x}) = \boldsymbol{c}\boldsymbol{x} \tag{4.5}$$

Note that $\boldsymbol{c}$ must satisfy the condition of rank($[\boldsymbol{c};\boldsymbol{c}\boldsymbol{N}]$)=2. From (4.2)–(4.5), the derivative of $s(\boldsymbol{x})$ with respective to time is

$$\dot{s}(\boldsymbol{x}) = \boldsymbol{c}(\boldsymbol{A}+u_0\boldsymbol{N})\boldsymbol{x} + u_{\mathrm{S}}\boldsymbol{c}\boldsymbol{N}\boldsymbol{x} = \lambda\, s(\boldsymbol{x}) + u_{\mathrm{S}}\boldsymbol{c}\boldsymbol{N}\boldsymbol{x} \tag{4.6}$$

Since $u\in\{-1, 1\}$, choose $u=-sgn(\rho(\boldsymbol{x}))\cdot sgn(s(\boldsymbol{x}))$, where $\rho(\boldsymbol{x})=\boldsymbol{c}\boldsymbol{N}\boldsymbol{x}$, and then u_{S} will be

$$u_{\mathrm{S}} = -u_0 + u = -u_0 - sgn(\rho(\boldsymbol{x}))\cdot sgn(s(\boldsymbol{x})) \tag{4.7}$$

From (4.5)–(4.7), we have

$$\begin{aligned} s(\boldsymbol{x})\dot{s}(\boldsymbol{x}) &= \lambda\, s(\boldsymbol{x})^2 + [-u_0 - sgn(\rho(\boldsymbol{x}))\cdot sgn(s(\boldsymbol{x}))]\cdot\rho(\boldsymbol{x})\cdot s(\boldsymbol{x}) \\ &= \lambda\, s(\boldsymbol{x})^2 - u_0\cdot\rho(\boldsymbol{x})\cdot s(\boldsymbol{x}) - sgn(\rho(\boldsymbol{x}))\cdot sgn(s(\boldsymbol{x}))\cdot\rho(\boldsymbol{x})\cdot s(\boldsymbol{x}) \\ &= \lambda\, s(\boldsymbol{x})^2 - [u_0\cdot sgn(\rho(\boldsymbol{x}))\cdot sgn(s(\boldsymbol{x})) + 1]\cdot|\rho(\boldsymbol{x})|\cdot|s(\boldsymbol{x})| \\ &= \lambda\, s(\boldsymbol{x})^2 - \alpha\cdot|\rho(\boldsymbol{x})|\cdot|s(\boldsymbol{x})| \\ &\le -\alpha\cdot|\rho(\boldsymbol{x})|\cdot|s(\boldsymbol{x})| \end{aligned} \tag{4.8}$$

where $\alpha=(1+u_0 \cdot sgn(\rho(\boldsymbol{x})) \cdot sgn(s(\boldsymbol{x})))$ and $0<\alpha<2$. Note that there are two features different from general sliding mode controls. First, u_S possesses two switching functions $sgn(\rho(\boldsymbol{x}))$ and $sgn(s(\boldsymbol{x}))$, *i.e.*, u_S will switch around two sets defined as $\Omega_s=\{\boldsymbol{x}|s(\boldsymbol{x})=0\}$ and $\Omega_N=\{\boldsymbol{x}|\rho(\boldsymbol{x})=0\}$. According to Assumption 4.2, $\boldsymbol{x}(t)$ will not belong to Ω_s and Ω_N simultaneously, except the equilibrium point $\boldsymbol{x}=\boldsymbol{0}$, and thus the state space can be well separated into four regions as shown in Fig. 4.1, in which u_S can be determined and it will switch when system trajectories pass through Ω_s or Ω_N.

Second, the equation (4.8) is similar to the RAS-condition (2.4), but the reaching rate in (4.8) is α multiplied with a state-dependent term $|\rho(\boldsymbol{x})|$. In general sliding mode controls, the system trajectories can be theoretically driven to the sliding mode only when the reaching rate is nonzero. However, in equation (4.8), $|\rho(\boldsymbol{x})|$ may always be zero (*i.e.*, once the system trajectory reach Ω_N, it will stay in Ω_N thereafter) such that the reaching rate is zero. With this observation, the reaching modes related to the state-dependent term $|\rho(\boldsymbol{x})|$ can be concluded into three types, as depicted in Fig. 4.2.

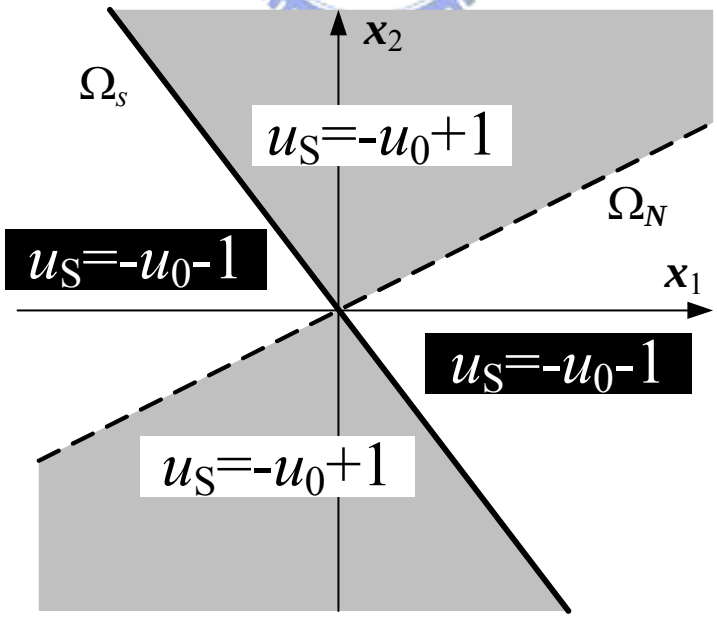

Fig. 4.1 Four regions in the state space separated by Ω_s and Ω_N.

For the reaching mode of type 1, without crossing Ω_N, the system trajectory starts from $\mathbf{p}_1$ and then reaches Ω_s at $\mathbf{p}_2$ in a finite time, which is the same as the reaching mode in general sliding controls. It is known that the equivalent control u_{eq} can be obtained as

$$\dot{s}\big|_{s=0,u_S=u_{eq}} = u_{eq} \cdot \boldsymbol{cNx} = u_{eq} \cdot \rho(\boldsymbol{x}) = 0 \tag{4.9}$$

Since the system trajectory stays in Ω_s and does not belong to Ω_N, u_{eq} will be zero, except the equilibrium point $\boldsymbol{x}=\mathbf{0}$. By substituting $u_S=u_{eq}=0$ into (4.3), the equivalent system dynamics becomes

$$\dot{\boldsymbol{x}} = \boldsymbol{A}_S \boldsymbol{x} \tag{4.10}$$

where $\boldsymbol{A}_S$ is stable. Therefore, the system (4.3) is stabilized once its system trajectory is constrained in the sliding mode.

For the reaching mode of type 2, the system trajectory starts from $\mathbf{q}_1$ and passes through Ω_N at $\mathbf{q}_2$ but not stay in Ω_N. After that, it reaches Ω_s at $\mathbf{p}_3$ in a finite time and then is stabilized with the same equivalent system dynamics as (4.10). Intuitively, when the system is switched from one subsystem to another subsystem through $\rho(\boldsymbol{x})=0$, the derivatives of $\rho(\boldsymbol{x})$ with respective to time for both subsystems must have the same sign. As discussed in §2.2, the switching behaviors around $\rho(\boldsymbol{x})=0$ are of the refractive mode and can be mathematically represented by (2.10). In other words, the reaching mode of type 2 is guaranteed if

$$\dot{\rho}(\boldsymbol{x})\big|_{\boldsymbol{A}_i=\boldsymbol{A}_1} \cdot \dot{\rho}(\boldsymbol{x})\big|_{\boldsymbol{A}_i=\boldsymbol{A}_2} > 0 \quad \text{for } \rho(\boldsymbol{x})=0 \text{ and } \boldsymbol{x} \neq \mathbf{0} \tag{4.11}$$

which is equivalent to

$$L_{\boldsymbol{A}_1\boldsymbol{x}}\rho(\boldsymbol{x}) \cdot L_{\boldsymbol{A}_2\boldsymbol{x}}\rho(\boldsymbol{x}) > 0 \quad \text{for } \rho(\boldsymbol{x})=0 \text{ and } \boldsymbol{x} \neq \mathbf{0} \tag{4.12}$$

Note that $L_{\boldsymbol{A}_1\boldsymbol{x}}\rho(\boldsymbol{x})$ and $L_{\boldsymbol{A}_2\boldsymbol{x}}\rho(\boldsymbol{x})$ are the directional derivatives of $\rho(\boldsymbol{x})$ with respective to the vector fields $\boldsymbol{A}_1\boldsymbol{x}$ and $\boldsymbol{A}_2\boldsymbol{x}$. That means the projections of $\boldsymbol{A}_1\boldsymbol{x}$ and $\boldsymbol{A}_2\boldsymbol{x}$ onto the gradient of $\rho(\boldsymbol{x})$ are in the same direction as shown in Fig. 4.3, in which ψ^+

and ψ^- denote the regions of $\{\boldsymbol{x}|\boldsymbol{cNA}_1\boldsymbol{x}>0,\ \boldsymbol{cNA}_2\boldsymbol{x}>0\}$ and $\{\boldsymbol{x}|\boldsymbol{cNA}_1\boldsymbol{x}<0,\ \boldsymbol{cNA}_2\boldsymbol{x}<0\}$, and they are bounded by two lines (L_1: $\boldsymbol{cNA}_1\boldsymbol{x}=0$ and L_2: $\boldsymbol{cNA}_2\boldsymbol{x}=0$). Clearly, if switching occurs inside the regions of ψ^+ and ψ^- (*i.e.*, (4.12) is satisfied), the system trajectories will pass through Ω_N. Such reaching mode is classified into type 2.

As for the reaching mode of type 3, the system trajectory starts from $\mathbf{r}_1$ and hits Ω_N at $\mathbf{r}_2$. Different from that of type 2, this system trajectory is constrained in Ω_N and $\boldsymbol{cNx}$ is always zero. From (4.6), the system dynamics is governed by

$$\dot{s} = \lambda\, s \tag{4.13}$$

such that the system trajectory cannot reach Ω_s in a finite time but exponentially approaches Ω_s instead, *i.e.*, this system trajectory will exponentially converge to the equilibrium point $\boldsymbol{x}=\boldsymbol{0}$, the intersection of Ω_s and Ω_N. Interestingly, the switching control (4.7) forces the system trajectories to switch along Ω_N, which means the switching motion along Ω_N is another sliding mode in this situation. Hence, the following inequality will be satisfied:

$$\dot{\rho}(\boldsymbol{x})\big|_{\rho(\boldsymbol{x})\to 0^+} < 0 \text{ and } \dot{\rho}(\boldsymbol{x})_{\rho(\boldsymbol{x})\to 0^-} > 0 \tag{4.14}$$

and it can be further written as

$$\begin{aligned}
&L_{A_2 x}\rho(\boldsymbol{x}) < 0, \text{ for } \rho(\boldsymbol{x}) = 0^+, s(\boldsymbol{x}) > 0\\
&L_{A_1 x}\rho(\boldsymbol{x}) > 0, \text{ for } \rho(\boldsymbol{x}) = 0^-, s(\boldsymbol{x}) > 0\\
&L_{A_1 x}\rho(\boldsymbol{x}) < 0, \text{ for } \rho(\boldsymbol{x}) = 0^+, s(\boldsymbol{x}) < 0\\
&L_{A_2 x}\rho(\boldsymbol{x}) > 0, \text{ for } \rho(\boldsymbol{x}) = 0^-, s(\boldsymbol{x}) < 0
\end{aligned} \tag{4.15}$$

Obviously, (4.15) express another sliding condition along Ω_N for $s(\boldsymbol{x})>0$ and $s(\boldsymbol{x})<0$.

From above, the bang-bang sliding mode control can theoretically stabilize the homogenous bilinear system (4.2). According to the switching input derived in (4.7), the switched system of (4.1) can be stabilized with the switching conditions as

$$\sigma(t) = \begin{cases} 1, & sgn(\boldsymbol{cNx})\cdot sgn(\boldsymbol{cx}) < 0 \\ 2, & sgn(\boldsymbol{cNx})\cdot sgn(\boldsymbol{cx}) > 0 \end{cases} \tag{4.16}$$

In this section, it shows that with Assumption 4.1 and Assumption 4.2 being satisfied, the bang-bang sliding mode control can be adopted to determine the

switching conditions for the switched systems consisting of two second-order unstable subsystems. In next section, it will be extended to another class of switched systems with model uncertainties.

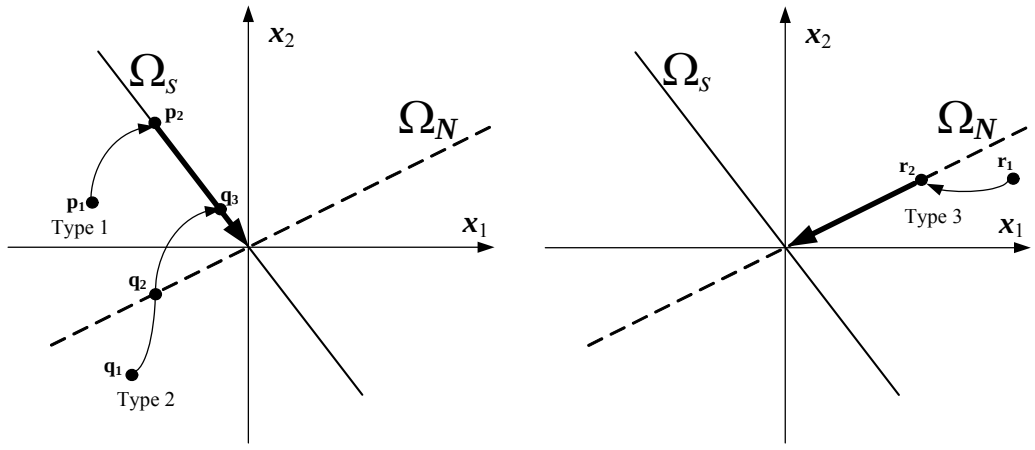

(a) (b)

Fig. 4.2 Three types of reaching modes.

(a) Reaching modes of type 1 and type 2. (b) Reaching mode of type 3.

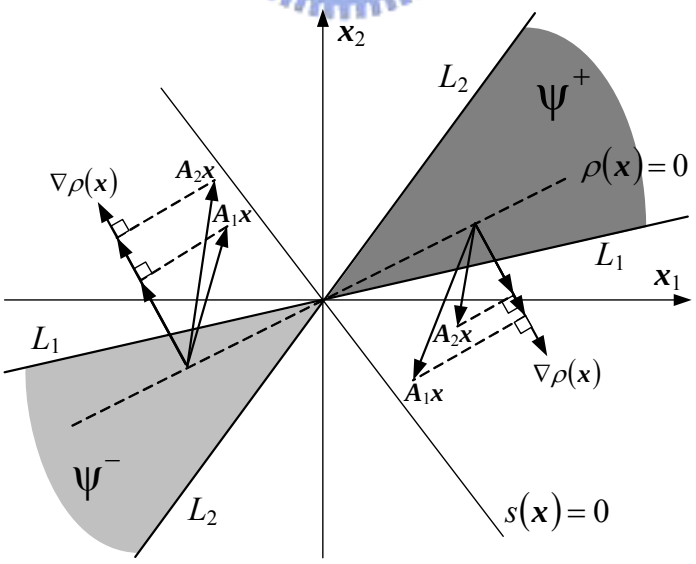

Fig. 4.3 Geometric representations of the directional derivatives for the reaching mode of type 2.

4.3 Stabilization of the Switched Systems with Model Uncertainties

As general sliding mode controls, the bang-bang sliding mode control is robust to model uncertainties in switched systems. Here, consider another class of switched systems containing model uncertainties, described by

$$\dot{\boldsymbol{x}} = \boldsymbol{A}_{\sigma(t)}\boldsymbol{x} + \Delta\boldsymbol{A}_{\sigma(t)}\boldsymbol{x} \tag{4.17}$$

where $\Delta\boldsymbol{A}_{\sigma(t)}$ are the model uncertainties and $\max_{\sigma(t)} \left\| \Delta\boldsymbol{A}_{\sigma(t)} \right\| \le \gamma$, γ is a constant. With Assumption 4.1 and Assumption 4.2, (4.17) can be expressed as

$$\dot{\boldsymbol{x}} = \boldsymbol{A}_S\boldsymbol{x} + u_S\boldsymbol{N}\boldsymbol{x} + \Delta\boldsymbol{A}_{\sigma(t)}\boldsymbol{x} \tag{4.18}$$

Obviously, the problem of designing a switching controller to stabilize (4.17) is changed into designing a robust switching controller for a homogenous bilinear system with state-dependent disturbance $\Delta\boldsymbol{A}_{\sigma(t)}\boldsymbol{x}$. Similar to the design procedures in §4.2, the equivalent control in the sliding mode can be derived from

$$u_{eq} \cdot \boldsymbol{c}\boldsymbol{N}\boldsymbol{x} + \boldsymbol{c}\Delta\boldsymbol{A}_{\sigma(t)}\boldsymbol{x} = 0 \tag{4.19}$$

Compared with (4.9), (4.19) contains $\boldsymbol{c}\Delta\boldsymbol{A}_{\sigma(t)}\boldsymbol{x}$ and thus u_{eq} may be affected by the model uncertainties. If $\boldsymbol{c}\Delta\boldsymbol{A}_{\sigma(t)}\boldsymbol{x}$ is zero in the sliding mode, u_{eq} will not be affected by the model uncertainties and is zero. However, in general cases, u_{eq} should be expressed as

$$u_{eq} = -\left(\boldsymbol{c}\boldsymbol{N}\boldsymbol{x}\right)^{-1} \cdot \boldsymbol{c}\Delta\boldsymbol{A}_{\sigma(t)}\boldsymbol{x} \tag{4.20}$$

Note that the existence of $(\boldsymbol{cNx})^{-1}$ is guaranteed in the sliding mode, except $\boldsymbol{x}=\boldsymbol{0}$. Substituting (4.20) into (4.18), the equivalent system dynamics will be

$$\dot{\boldsymbol{x}} = \boldsymbol{A}_S\boldsymbol{x} - \left(\boldsymbol{c}\boldsymbol{N}\boldsymbol{x}\right)^{-1} \cdot \boldsymbol{c}\Delta\boldsymbol{A}_{\sigma(t)}\boldsymbol{x} \cdot \boldsymbol{N}\boldsymbol{x} + \Delta\boldsymbol{A}_{\sigma(t)}\boldsymbol{x} \tag{4.21}$$

Assume that the norm of $\boldsymbol{N}$ is bounded by a constant β (*i.e.*, $\left\|\boldsymbol{N}\right\| \le \beta$), and choose a symmetric positive-definite matrix $\boldsymbol{P}$ such that $\boldsymbol{x}^T\boldsymbol{P}\boldsymbol{x}$ is a candidate of Lyapunov function, which is denoted as V. Then, the derivative of V with respective to time can be obtained as

$$\begin{aligned}\dot{V} &= \boldsymbol{x}^T\left(\boldsymbol{A}_S{}^T\boldsymbol{P}+\boldsymbol{P}\boldsymbol{A}_S\right)\boldsymbol{x}-\left(\boldsymbol{c}\boldsymbol{N}\boldsymbol{x}\right)^{-1}\cdot\boldsymbol{c}\Delta\boldsymbol{A}_{\sigma(t)}\boldsymbol{x}\cdot\boldsymbol{x}^T\left(\boldsymbol{N}^T\boldsymbol{P}+\boldsymbol{P}\boldsymbol{N}\right)\boldsymbol{x}\\ &\quad+\boldsymbol{x}^T\left(\Delta\boldsymbol{A}_{\sigma(t)}{}^T\boldsymbol{P}+\boldsymbol{P}\Delta\boldsymbol{A}_{\sigma(t)}\right)\boldsymbol{x}\\ &\le-\boldsymbol{x}^T\boldsymbol{Q}\boldsymbol{x}+\left|\frac{\boldsymbol{c}\Delta\boldsymbol{A}_{\sigma(t)}\boldsymbol{x}}{\boldsymbol{c}\boldsymbol{N}\boldsymbol{x}}\right|2\beta\|\boldsymbol{P}\|\|\boldsymbol{x}\|^2+2\gamma\|\boldsymbol{P}\|\|\boldsymbol{x}\|^2 \qquad (4.22)\\ &\le-\boldsymbol{x}^T\boldsymbol{Q}\boldsymbol{x}+\left|\frac{\phi_{\sigma(t)}(\boldsymbol{x})}{\rho(\boldsymbol{x})}\right|2\beta\|\boldsymbol{P}\|\|\boldsymbol{x}\|^2+2\gamma\|\boldsymbol{P}\|\|\boldsymbol{x}\|^2\end{aligned}$$

where $\boldsymbol{Q}$ is a symmetric positive-definite matrix and $\phi_{\sigma(t)}(\boldsymbol{x})=\boldsymbol{c}\Delta\boldsymbol{A}_{\sigma(t)}\boldsymbol{x}$. Besides, it is known that

$$\lambda_{min}(\boldsymbol{Q})\|\boldsymbol{x}\|^2\le\boldsymbol{x}^T\boldsymbol{Q}\boldsymbol{x}\le\lambda_{max}(\boldsymbol{Q})\|\boldsymbol{x}\|^2 \qquad (4.23)$$

where $\lambda_{min}(\cdot)$ and $\lambda_{max}(\cdot)$ denote the minimum eigenvalue and maximum eigenvalue of a matrix respectively. Further, for some $\boldsymbol{x}_s$ in the sliding mode, define $max|\phi_{\sigma(t)}(\boldsymbol{x}_s)|$ and $|\rho(\boldsymbol{x}_s)|$ as l_Δ and l_N, and denote the ratio of l_Δ to l_N as l, which are shown in Fig. 4.4 in the geometric view.

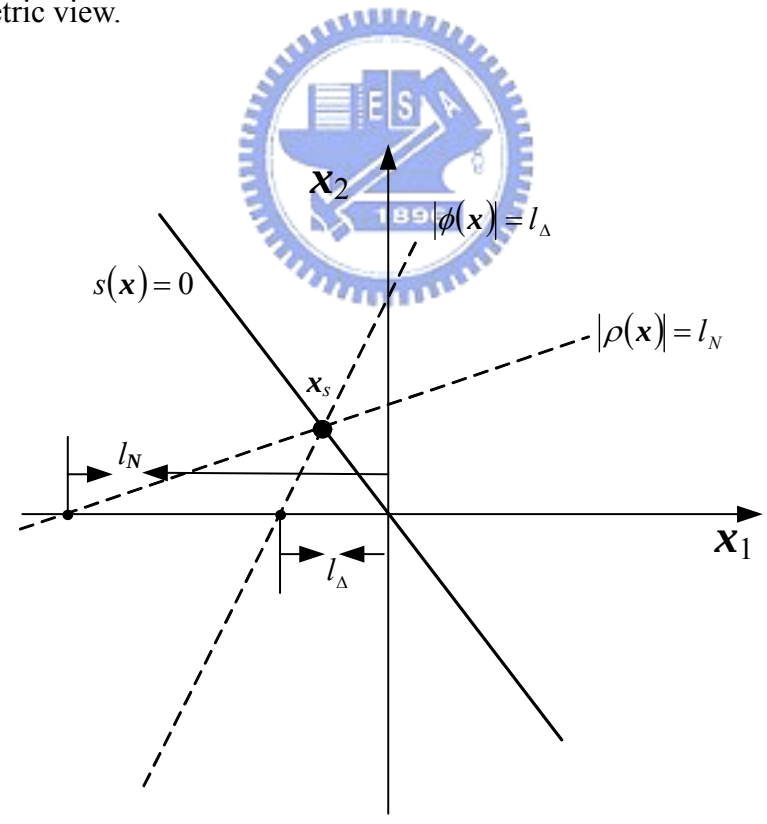

Fig. 4.4 Geometric view of l_N and l_Δ related to model uncertainties.

Substituting l_N, l_Δ and l into (4.22), it leads to

$$\dot{V} \le -\left(\lambda_{min}(\boldsymbol{Q}) - 2\beta \cdot l \cdot \|\boldsymbol{P}\| - 2\gamma\|\boldsymbol{P}\|\right)\|\boldsymbol{x}\|^2 \tag{4.24}$$

Note that l is a constant value for all the $\boldsymbol{x}_s$ in the sliding mode and it is finite since Assumption 4.2 is satisfied, *i.e.*, $|\rho(\boldsymbol{x}_s)|$ is nonzero, except $\boldsymbol{x}_s$=$\boldsymbol{0}$. Thus, it can be concluded that V is a Lyapunov function if the following inequality is satisfied

$$\frac{\lambda_{min}(\boldsymbol{Q})}{2\|\boldsymbol{P}\|} - \beta \cdot l - \gamma > 0 \tag{4.25}$$

and it yields $\boldsymbol{x}(t) \rightarrow \boldsymbol{0}$ as $t \rightarrow \infty$.

From above, the stability of the switched system is guaranteed in the sliding mode if (4.25) is satisfied. However, it still needs to check the reaching condition for the switched system since the model uncertainties also affect the original reaching rate. Similar to (4.8), the reaching condition for the switched system with model uncertainties is

$$-\left(|\lambda| \cdot |s(\boldsymbol{x})| + \alpha \cdot |\rho(\boldsymbol{x})| - |\phi_{\sigma(t)}(\boldsymbol{x})|\right) \cdot |s(\boldsymbol{x})| \le -\sigma \cdot |\rho(\boldsymbol{x})| \cdot |s(\boldsymbol{x})| \tag{4.26}$$

where σ is some positive constant. Obviously, there are three state-dependent terms related to the reaching rate and the RAS-condition can be guaranteed only when (4.26) is satisfied for all $\boldsymbol{x}$ in $\boldsymbol{R}^2$, except $\boldsymbol{x}$=$\boldsymbol{0}$. While Assumption 4.2 is satisfied, $\boldsymbol{c}\Delta\boldsymbol{A}_i$ can be represented in the linear combination of $\boldsymbol{c}$ and $\boldsymbol{cN}$ as

$$\boldsymbol{c}\Delta\boldsymbol{A}_i = w_{s,i}\boldsymbol{c} + w_{\rho,i}\boldsymbol{cN} \tag{4.27}$$

where $w_{s,i}$ and $w_{\rho,i}$ are the coefficients of i-th model uncertainty represented by vectors $\boldsymbol{c}$ and $\boldsymbol{cN}$. With two model uncertainties in the switched system, the reaching rate can be expressed as

$$\left(|\lambda| - |w_{s,i}|\right) \cdot |s(\boldsymbol{x})| + \left(\alpha - |w_{\rho,i}|\right) \cdot |\rho(\boldsymbol{x})|, \; i = 1, 2 \tag{4.28}$$

Clearly, if $w_{s,i}$ and $w_{\rho,i}$ are bounded by

$$|w_{s,i}| < |\lambda|, \; i = 1, 2 \tag{4.29}$$

and

$$|w_{\rho,i}| < \alpha, \; i = 1, 2 \tag{4.30}$$

(4.26) is satisfied and the system trajectories will reach the sliding mode in a finite

time. Note that α takes two possible values of $1-u_0$ and $1+u_0$, and the minimum value of α is obtained as $1-|u_0|$, which is used to check (4.30). Besides, there may also exist the reaching mode of type 3 with the system dynamics described by (4.13). While (4.29) is satisfied, the system trajectory can still exponentially converge to the equilibrium point $\boldsymbol{x}=\mathbf{0}$.

From above, it shows that the proposed switching controller is robust to the model uncertainties if (4.25) and (4.26) (or, (4.29) and (4.30)) are both satisfied. In next section, numerical simulations will be given to demonstrate the effectiveness of the proposed bang-bang sliding mode control.

4.4 Numerical Simulation Results

In this section, several examples are given to show the cases discussed in §4.2 and §4.3. First, three possible reaching modes under the bang-bang sliding mode control are illustrated in example 4.1 (with reaching modes of type 1 or type 2), and example 4.2 (with reaching modes of type 1 or type 3). Finally, a switched system with model uncertainties is considered in example 4.3.

Example 4.1:

Consider the second-order switched system given in [34], which consists of two unstable subsystems expressed as

$$\boldsymbol{A}_1 = \begin{bmatrix} -4 & -5 \\ 7 & 7 \end{bmatrix} \quad \boldsymbol{A}_2 = \begin{bmatrix} 3 & 5 \\ -7 & -13 \end{bmatrix} \tag{4.31}$$

where the eigenvalues of $\boldsymbol{A}_1$ and $\boldsymbol{A}_2$ are $\{1.5+i2.1794,\ 1.5-i2.1794\}$ and $\{0.3852,\ -10.3852\}$ respectively. First, rewrite (4.31) into a second-order homogenous bilinear system as

$$\dot{\boldsymbol{x}} = \boldsymbol{A}\boldsymbol{x} + u\boldsymbol{N}\boldsymbol{x} = \begin{bmatrix} -0.5 & 0 \\ 0 & -3 \end{bmatrix}\boldsymbol{x} + u\begin{bmatrix} -3.5 & -5 \\ 7 & 10 \end{bmatrix}\boldsymbol{x} \tag{4.32}$$

and choose u_0 as 0.09. Then, Assumption 4.1 is satisfied since $\boldsymbol{A}\boldsymbol{x}+u_0\boldsymbol{N}\boldsymbol{x}$ has stable eigenvalues $\lambda_1=-1.0979$ and $\lambda_2=-1.8171$ with left eigenvectors $\boldsymbol{c}_1=[0.9122\ -0.4097]$ and $\boldsymbol{c}_2=[-0.5322\ \ 0.8466]$ correspondingly. Assumption 4.2 is also satisfied by checking rank$[\boldsymbol{c}_1;\boldsymbol{c}_1\boldsymbol{N}]=2$. Therefore, the sliding function can be chosen as $\boldsymbol{c}_1\boldsymbol{x}$ and from (4.16), the switching conditions of (4.31) can be obtained as

$$\sigma(t) = \begin{cases} 1, & sgn(-6.0604x_1 - 8.6577x_2)\cdot sgn(0.9122x_1 - 0.4097x_2) < 0 \\ 2, & sgn(-6.0604x_1 - 8.6577x_2)\cdot sgn(0.9122x_1 - 0.4097x_2) > 0 \end{cases} \tag{4.33}$$

Under the switching conditions (4.33), the simulation results of (4.31) are shown in Fig. 4.5 including four possible system trajectories. For the system trajectories starting from $[0.5\ 0.5]^T$ and $[-0.5\ -0.5]^T$, they reach the sliding mode Ω_s in a finite time without crossing Ω_N, which shows the reaching mode of type 1. As for the system trajectories starting from $[-0.5\ 0.5]^T$ and $[0.5\ -0.5]^T$, they present the reaching mode of type 2, passing through Ω_N and then reaching the sliding mode Ω_s. For all these system trajectories, once they are in the sliding mode Ω_s, they will always stay in it and move toward the equilibrium point $\boldsymbol{x}=\boldsymbol{0}$.

Remark 4.1:

For the system trajectories with reaching mode of type 2, (4.12) must be satisfied. This can be easily verified by substituting $\boldsymbol{x}_N=[\eta\ \ -0.7\eta]^T$, where $\boldsymbol{x}_N \in \Omega_N$ and $\eta \in R$, into $\boldsymbol{cNA}_1\boldsymbol{x}$ and $\boldsymbol{cNA}_2\boldsymbol{x}$. For any nonzero η, we have

$$L_{A_1 x}\rho(\boldsymbol{x}_N)\cdot L_{A_2 x}\rho(\boldsymbol{x}_N) = \boldsymbol{cNA}_1\boldsymbol{x}_N \cdot \boldsymbol{cNA}_2\boldsymbol{x}_N = 229.5536\eta^2 > 0 \tag{4.34}$$

which guarantees (4.12). Thus, for the system trajectories reaching Ω_N, they will pass through Ω_N and such reaching mode is classified into type 2 and only stable sliding motions exist in this switched system.

Example 4.2:

Consider a second-order switched system, consisting of two unstable subsystems given as

$$\boldsymbol{A}_1 = \begin{bmatrix} 0.7 & -2 \\ -3.65 & 4.8 \end{bmatrix} \quad \boldsymbol{A}_2 = \begin{bmatrix} -1.3 & 2 \\ 2.35 & 3.2 \end{bmatrix} \tag{4.35}$$

where the eigenvalues of $\boldsymbol{A}_1$ and $\boldsymbol{A}_2$ are $\{-0.6415,\ 0.6145\}$ and $\{0.117,\ -4.617\}$ respectively. First, rewrite (4.35) into a second-order homogenous bilinear system as

$$\dot{\boldsymbol{x}} = \boldsymbol{A}\boldsymbol{x} + u\boldsymbol{N}\boldsymbol{x} = \begin{bmatrix} -0.3 & 0 \\ -0.65 & 0.8 \end{bmatrix}\boldsymbol{x} + u\begin{bmatrix} 1 & -2 \\ -3 & 4 \end{bmatrix}\boldsymbol{x} \tag{4.36}$$

and choose u_0 as −0.3. Then, Assumption 4.1 is satisfied since $\boldsymbol{Ax}+u_0\boldsymbol{Nx}$ has stable eigenvalues λ_1=−0.1 and λ_2=−0.9 with left eigenvectors $\boldsymbol{c}_1$=[−0.4472 −0.8944] and $\boldsymbol{c}_2$=[−0.6402 0.7682] correspondingly. Assumption 4.2 is also satisfied by checking rank[$\boldsymbol{c}_1$;$\boldsymbol{c}_1\boldsymbol{N}$]=2. Therefore, the sliding function s can be chosen as $\boldsymbol{c}_1\boldsymbol{x}$ and from (4.16), the switching conditions of (4.35) can be obtained as

$$\sigma(t)=\begin{cases} 1, & sgn(-2.2361x_1-2.6683x_2)\cdot sgn(-0.4472x_1-0.8944x_2)<0 \\ 2, & sgn(-2.2361x_1-2.6683x_2)\cdot sgn(-0.4472x_1-0.8944x_2)>0 \end{cases} \tag{4.37}$$

Under the switching conditions (4.37), the simulation results of (4.35) are shown in Fig. 4.6 including four possible system trajectories. Different from example 4.1, the system trajectories may stay in Ω_s or Ω_N, depending on which sliding mode that the system trajectories reach first. For the system trajectories starting from $[-0.5\ 0.5]^T$ and $[0.5\ -0.5]^T$, they reach Ω_s first, presenting the reaching mode of type 1. For the system trajectories starting from $[0.2\ 0.8]^T$ and $[-0.2\ -0.8]^T$, they reach Ω_N first and then stay in it. Although the system trajectories cannot reach Ω_s, they truly slide along Ω_N and converge to $\boldsymbol{x}$=0 exponentially as described in §4.3. Clearly, for all these system trajectories, they will stay in the sliding mode Ω_s or Ω_N, and move toward the equilibrium point $\boldsymbol{x}$=**0**.

Remark 4.2:

For the system trajectories sliding along Ω_N, the inequalities in (4.15) must be satisfied, which can be verified by the following process. First, under the condition of $\rho(\boldsymbol{x})$ being around zero, assume $s(\boldsymbol{x})=\tau$ and $\rho(\boldsymbol{x})=\delta$, where τ is a nonzero number and $\delta\to 0$. Then, we have

$$\begin{bmatrix} s(\boldsymbol{x}) \\ \rho(\boldsymbol{x}) \end{bmatrix}=\begin{bmatrix} \boldsymbol{c} \\ \boldsymbol{cN} \end{bmatrix}\boldsymbol{x}=\begin{bmatrix} -0.4472 & -0.8944 \\ 2.2361 & -2.6833 \end{bmatrix}\boldsymbol{x}=\begin{bmatrix} \tau \\ \delta \end{bmatrix} \tag{4.38}$$

Since Assumption 4.2 is satisfied, the square matrix in (4.38) is invertible and the solution of $\boldsymbol{x}$ can be obtained as

$$\boldsymbol{x}=\begin{bmatrix}\boldsymbol{c}\\ \boldsymbol{cN}\end{bmatrix}^{-1}\begin{bmatrix}\tau\\ \delta\end{bmatrix}=\begin{bmatrix}-0.8385\tau+0.2795\delta\\ -0.6988\tau-0.1398\delta\end{bmatrix} \tag{4.39}$$

Further, by substituting the $\boldsymbol{x}$ in (4.39) into $L_{\boldsymbol{A}_1\boldsymbol{x}}\rho(\boldsymbol{x})$ and $L_{\boldsymbol{A}_2\boldsymbol{x}}\rho(\boldsymbol{x})$, it results in

$$L_{\boldsymbol{A}_1\boldsymbol{x}}\rho(\boldsymbol{x})=\boldsymbol{cNA}_1\begin{bmatrix}\boldsymbol{c}\\ \boldsymbol{cN}\end{bmatrix}^{-1}\begin{bmatrix}\tau\\ \delta\end{bmatrix}=2.6\tau+5.6\delta \tag{4.40}$$

and

$$L_{\boldsymbol{A}_2\boldsymbol{x}}\rho(\boldsymbol{x})=\boldsymbol{cNA}_2\begin{bmatrix}\boldsymbol{c}\\ \boldsymbol{cN}\end{bmatrix}^{-1}\begin{bmatrix}\tau\\ \delta\end{bmatrix}=-1.4\tau-4.4\delta \tag{4.41}$$

Hence,

$$\begin{aligned}
&L_{\boldsymbol{A}_2\boldsymbol{x}}\rho(\boldsymbol{x})=-1.4\tau+\delta<0 \quad \text{for } \rho(\boldsymbol{x})=\delta>0, s(\boldsymbol{x})=\tau>0\\
&L_{\boldsymbol{A}_1\boldsymbol{x}}\rho(\boldsymbol{x})=\ 2.6\tau+\delta>0 \quad \text{for } \rho(\boldsymbol{x})=\delta<0, s(\boldsymbol{x})=\tau>0\\
&L_{\boldsymbol{A}_1\boldsymbol{x}}\rho(\boldsymbol{x})=\ 2.6\tau+\delta<0 \quad \text{for } \rho(\boldsymbol{x})=\delta>0, s(\boldsymbol{x})=\tau<0\\
&L_{\boldsymbol{A}_2\boldsymbol{x}}\rho(\boldsymbol{x})=-1.4\tau+\delta>0 \quad \text{for } \rho(\boldsymbol{x})=\delta<0, s(\boldsymbol{x})=\tau<0
\end{aligned} \tag{4.42}$$

This verifies (4.15) and Ω_N is really a sliding mode in this example.

Example 4.3:

Consider the switched system given in example 4.1 again but containing the model uncertainties $\Delta\boldsymbol{A}_{\sigma(t)}$ with the values of

$$\Delta\boldsymbol{A}_1=\begin{bmatrix}0.15 & 0.3\\ 0.45 & 0.15\end{bmatrix},\ \Delta\boldsymbol{A}_2=-\begin{bmatrix}0.12 & 0.25\\ 0.4 & 0.1\end{bmatrix}$$

Then, it can be obtained that $\gamma=max(\|\Delta\boldsymbol{A}_1\|,\|\Delta\boldsymbol{A}_2\|)=0.5427$ and $\|\boldsymbol{N}\|=\beta=13.6473$. When a $\boldsymbol{Q}$ is given, a corresponding $\boldsymbol{P}$ can be obtained by Matlab software, *e.g.*,

$$\boldsymbol{P}=\begin{bmatrix}0.6189 & 0.0070\\ 0.0070 & 0.4747\end{bmatrix},\ \boldsymbol{Q}=\begin{bmatrix}1 & 0\\ 0 & 2\end{bmatrix} \tag{4.43}$$

with $\lambda_{min}(\boldsymbol{Q})=1$ and $\|\boldsymbol{P}\|=0.6193$. Further, let $\boldsymbol{x}_s=[\eta\ \ 2.2269\eta]^T$, where $\boldsymbol{x}_s\in\Omega_s$ and $\eta\in R$, we can obtain that $l_N=25.3401\eta$, $l_\Delta=0.4251\eta$ and $l=0.0168$. Then, (4.25) is satisfied from the following calculation:

$$\begin{aligned}
\frac{\lambda_{min}(\boldsymbol{Q})}{2\|\boldsymbol{P}\|}-\beta\cdot l-\gamma&=\frac{1}{1.2386}-13.6437\cdot 0.0168-0.5427\\
&=0.0356>0
\end{aligned} \tag{4.44}$$

which guarantees that the switched system is robust to the model uncertainties in the sliding mode. Next, check the reaching condition in (4.26) and the coefficients in (4.27) can be obtained as $w_{s,1}$=–0.1635, $w_{\rho,1}$=–0.0168, $w_{s,2}$=0.1546 and $w_{\rho,2}$=0.0143. Obviously, (4.29) can be satisfied by checking:

$$\left|w_{s,i}\right| < \left|\lambda\right| = 1.0979 \ , \ \left|w_{\rho,i}\right| < \alpha = 0.91, \ i = 1, 2 \tag{4.45}$$

Therefore, the reaching condition is also satisfied in the presence of model uncertainties. Then, the switching conditions in (4.37) can be used to stabilize the switched system and the system trajectories in the numerical simulation are shown in Fig. 4.7.

In this example, it shows that the bang-bang sliding mode control can stabilize the second-order switched system with model uncertainties if (4.25) and (4.26) are satisfied for the mode uncertainties.

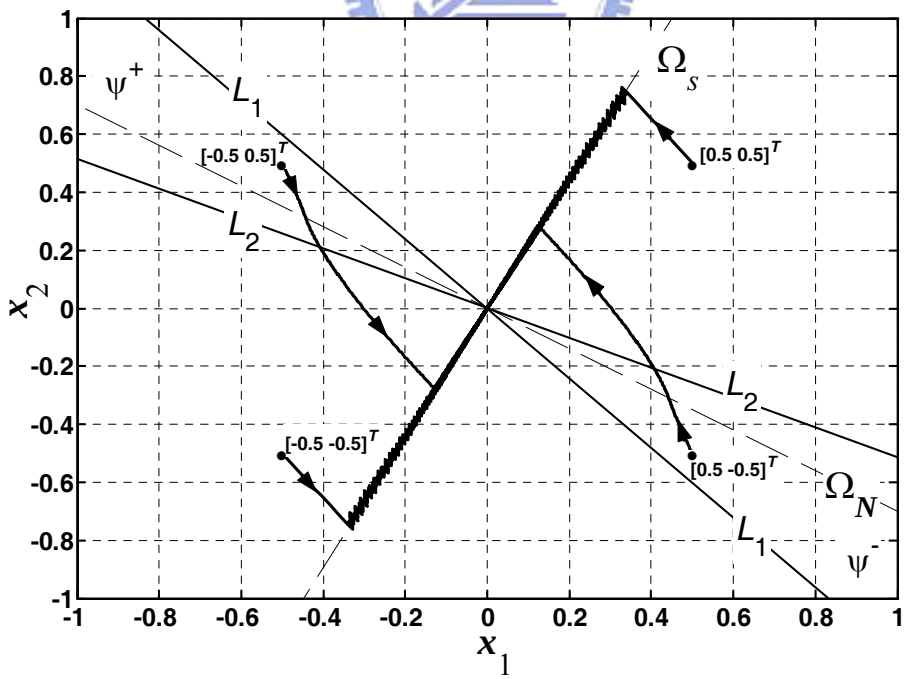

Fig. 4.5 System trajectories of example 4.1: reaching modes of type 1 and type 2.

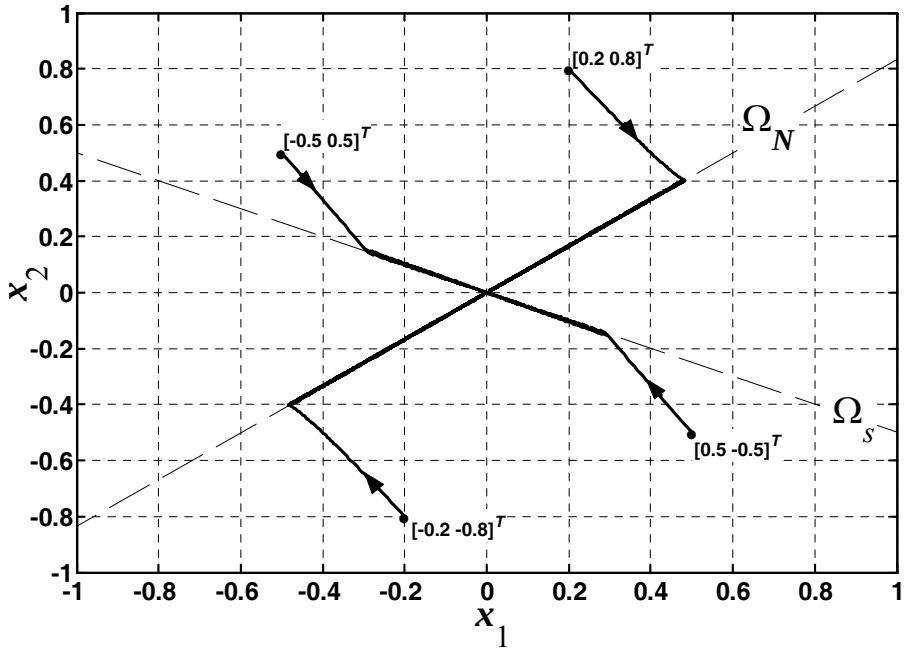

Fig. 4.6 System trajectories of example 4.2: reaching modes of type 1 and type 3.

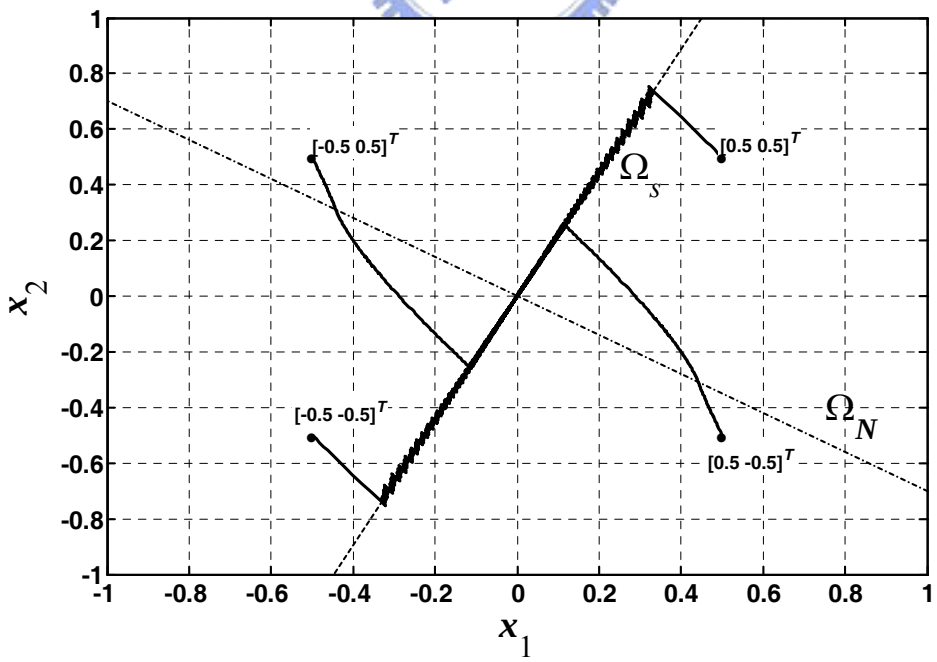

Fig. 4.7 System trajectories of example 4.3.

Chapter 5 Conclusion and Future Work

5.1 Conclusion

This dissertation is devoted to design the switching controller for a buck DC-DC converter and stabilize a class of switched systems based on the bang-bang sliding mode control. The basic theorems related to the bang-bang sliding mode control are first introduced in Chapter 2 and then, three modes of switching motions around the switching surface are described. The contributions of this dissertation are summarized as follows.

In Chapter 3, the design procedures of the bang-bang sliding mode control for a buck DC-DC converter are given. The system trajectories are clearly depicted in the phase plane and their RAS-regions are analyzed in detail with respect to different sliding functions. The experimental results obtained from the prototype hardware are demonstrated and the buck DC-DC converter is shown to be robust to resistive load variations. Besides, some modifications of the original bang-bang sliding mode control are included for the practical implementation. The purpose of operating the converter at a constant switching frequency is achieved by incorporating a periodic ramp signal and a PI-type compensator. In the simulation results, it shows that the buck DC-DC converter can ideally operate at a constant switching frequency invariant to operation points and the steady-state errors resulting from the nonzero averaging value of sliding function can be eliminated by the compensator.

In Chapter 4, the bang-bang sliding mode control is extended to design the switching controller for a class of switched systems consisting of two unstable second-order subsystems. Two important assumptions are derived for the existence of stable sliding motions. Three types of reaching modes are clearly discussed and

verified by numerical simulation results. Besides, a switched system with model uncertainties is considered and we show that the bang-bang sliding mode control is robust in the presence of model uncertainties. Compared with other methods, the bang-bang sliding mode control only consists of the state-static-memoryless feedback laws and thus it can be easily realized.

5.2 Future Work

In this dissertation, it shows that the bang-bang sliding mode control is effective in designing the switching controllers for buck DC-DC converters and a specific class of switched systems. Nevertheless, there still exist some issues worthy of further studies. In Chapter 3, the work of determining the coefficients of the sliding function and the PI-type compensator are separated in two independent steps. However, it can integrate these steps into one step by designing the original sliding function with the integral term of output voltage error. Without separately designing the sliding function and the PI-type compensator, the overall system dynamics in the sliding mode can be properly assigned and it can be referred to the work in [20].

A unified approach has been proposed to design the PWM-based sliding mode voltage controllers for boost and buck-boost DC-DC converters [22]. However, it is still difficult to design a static sliding mode without the integral term. Therefore, the work in Chapter 4 has the potentiality of being extended to the converters having un-negligible bilinear terms in their large-signal models.

The existence of stable sliding motions in Chapter 4 is only guaranteed for second-order switched systems. However, for high-order switched system, there may exist unstable hyper-switching motions, *i.e.*, the system trajectories switch along both of $s(\boldsymbol{x})=0$ and $\rho(\boldsymbol{x})=0$, and then become unstable. In order to apply the bang-bang

sliding mode control in high-order switched systems, the conditions for the existence of stable hyper-switching motion and the exclusion of hyper-switching motion are both deserving of further research.

Bibliography

1. V. I. Utkin, *Sliding Regimes and Their Applications in Variable Structure Systems*, MIR, Moscow, 1978.
2. J.-J. E. Slotine and W. Li, *Applied Nonlinear Control*, Ch. 7, Prentice-Hall, New York, 1991.
3. R. A. DeCarlo, S. H. Zak and G. P. Mattews, "Variable structure control of nonlinear multivariable systems: a tutorial," *IEEE Proc.*, Vol. 76, No. 3, pp. 212–232, 1988.
4. J. Y. Huang, W. Gao, and J. C. Hung, "Variable structure control: a survey," *IEEE Trans. on Ind. Electron.*, Vol. 40, No. 1, pp. 2–22, 1993.
5. W. Gao and J. C. Hung, "Variable structure control of nonlinear systems: a new approach," *IEEE Trans. on Ind. Electron.*, Vol. 40, No. 1, pp. 45–55, 1993.
6. K. D. Young, V. I. Utkin, and U. Ozguner, "A control engineer's guide to sliding mode control," *IEEE Trans. on Cont. Syst. Technol.*, Vol. 7, No. 3, pp. 328–342, 1999.
7. V. I. Utkin, J. Guldner, and J. Shi, *Sliding Mode Control in Electromechanical Systems*, Taylro & Francis Press, London, 1999.
8. W. Perruquetti and J.-P. Barbot, *Sliding Mode Control in Engineering*, Marcel Dekker, New York, 2002.
9. A. Sabanovic, N. Sabanovic, and K. Ohnishi, "Sliding modes in power converters and motion control systems," *Int. J. of Cont.*, Vol. 57, No. 5, pp. 1237–1259, 1993.
10. A. Sabanovic, K. Jezernik, and N. Sabanovic, *Variable Structure Systems: Towards the 21st Century*, LNCIS, Vol. 274, pp. 223–251, 2002.
11. R.R. Mohler, *Nonlinear Systems, Volume II, Applications to Bilinear Control*,

Prentice-Hall, New York, 1991.

12. H. Sira-Ramirez, “Sliding motions in bilinear switched networks”, *IEEE Trans. on Circuits and Syst.*, Vol. 34, No. 8, pp. 919–933, 1987.
13. Yon-Ping Chen, Jeang-Lin Chang, and Kuo-Ming Lai, “Stability Analysis and Bang–Bang Sliding Control Class of Single-Input Bilinear Systems,” *IEEE Trans. on Auto. Cont.*, Vol. 45, No. 11, pp. 2150–2154, 2000.
14. H. Sira-Ramirez, “Differential geometric methods in variable structure control,” *Int. J. of Cont.*, Vol. 48, No. 4, pp. 1359–1391, 1988.
15. H. Sira-Ramirez and M. Ilic, “A geometric approach to the feedback control of switch mode dc-to-dc power supplies”, *IEEE Trans. on Circuits and Syst.*, Vol. 35, No. 10, pp. 1291–1298, 1988.
16. R.O. Caceres and I. Barbi, “A Boost DC-AC Converter: Analysis, Design, and Experimentation,” *IEEE Trans. on Power Electron.*, Vol. 14, No. 1, pp. 134–141, 1999.
17. M. Carpita and M. Marchesoni, “Experimental study of a power conditioning system using sliding mode control”, *IEEE Trans. on Power Electon.*, Vol. 11, No. 5, pp. 731–742, 1996.
18. G. Escobar, R. Ortega, H. Sira-Ramirez, J.P. Vilain, and I. Zein, “An experimental comparison of several nonlinear controllers for power converters”, *IEEE Cont. Syst. Magazine*, Vol. 19, pp. 66–82, 1999.
19. S. C. Tan, Y. M. Lai, M. K. H. Cheung, and C. K. Tse, “On the practical design of a sliding mode voltage controlled buck converter,” *IEEE Trans. on Power Electron.*, Vol. 20, No. 2, pp. 425–437, 2005.
20. S. C. Tan, Y. M. Lai, C. K. Tse, and M. K. H. Cheung, “A fixed-frequency pulsewidth modulation based quasi-sliding-mode controller for buck converters,” *IEEE Trans. on Power Electron.*, Vol. 20, No. 6, pp. 1379–1392, 2005.

21. S. C. Tan, Y. M. Lai, C. K. Tse, and M. K. H. Cheung, “Adaptive feedforward and feedback control schemes for sliding mode controlled power converters,” *IEEE Trans. on Power Electron*., Vol. 21, No. 1, pp. 182–192, 2006.
22. S. C. Tan, M. K. H. Cheung, C. K. Tse, and Y. M. Lai, “A unified approach to the design of PWM-based sliding-mode voltage controllers for basic DC-DC converters in continuous conduction mode,” *IEEE Trans. on Circuits and Syst.–I*, Vol. 53, No. 8, pp. 1816–1827, 2006.
23. Y. He and F. L. Luo, “Sliding-mode control for dc-dc converters with constant switching frequency,“ *IEE Proc. on Cont. Theory and Applicat.*, Vol. 153, pp. 37–45, 2006.
24. Y. He and F. L. Luo, “Design and analysis of adaptive sliding-mode-like controller for DC-DC converters,“ *IEE Proc. on Cont. Theory and Applicat.*, Vol. 153, pp. 401–410, 2006.
25. P. Mattavelli, L. Rossetto, G. Spiazzi, and P. Tenti, "General-purpose sliding-mode controller for DC/DC converter applications, " Proc. of IEEE Power Electronics Specialists Conf. (PESC), pp. 609–615, 1993.
26. G. Spiazzi, P. Mattavelli, and L. Rossetto, "Sliding-mode control of dc-dc converters, " IEEE 4th Brasilian Power Electronics Conf. (COBEP), pp. 59–68, 1997.
27. N. Mohan, T. M. Undeland, and W. P. Robbins, *Power Electronics: Converters, Applications, and Design*, *2nd edn*, John Wiley & Sons, New York, 1995.
28. S. C'uk and R. D. Middlebrook, "A general unified approach to modeling switching DC-to-DC converters in discontinuous conduction mode," Proc. of IEEE Power Electronics Specialists Conf. (PESC), pp. 18–34, 1977.
29. P. Gupta and A. Patra, “Hybrid Mode-Switched Control of DC-DC Boost Converter Circuits, ” *IEEE Trans. on Circuit and Syst.–II*, Vol. 52, No. 11,

pp.734–738, 2005.

30. R. Leyva, L. Martínez-Salamero, H. Valderrama-Blavi, J. Maixé, R. Giral, and F. Guinjoan, "Linear State-Feedback Control of a Boost Converter for Large-Signal Stability, " *IEEE Trans. on Circuit and Syst.–I*, Vol. 48, No. 4, pp. 418-424, 2001.
31. Daniel Liberzon, *Switching in Systems and Control*, Birkhauser, Boston, 2003.
32. D. Liberzon and A. S. Morse, "Basic problems in stability and design of switched systems," *IEEE Contr. Syst. Magazine*, Vol. 19, No. 5, pp. 59–70, 1999.
33. M. A. Wicks, P. Peleties, and R. DeCarlo, "Construction of piecewise Lyapunov functions for stabilizing switched systems," *Proc. 33rd IEEE Conf. Decision Cont.*, Lake Buena Vista, FL, pp. 3492–3497, 1994.
34. M. A. Wicks, P. Peleties, and R. DeCarlo, "Switched controller synthesis for the quadratic stabilization of a pair of unstable linear systems," *European J. of Cont.*, Vol. 4, No. 2, pp. 140–147, 1998.
35. R. A. Decarlo, M. S. Branicky, S. Pettersson, and B. Lennartson, "Perspectives and results on the stability and stabilizability of hybrid systems," *IEEE Proc.*, Vol. 88, No. 7, pp. 1069–1082, 2000.
36. X. Xu and P.J. Antasklis, "Stabilization of second-order LTI switched systems," *Int. J. of Cont.*, Vol. 73, No. 14, pp. 1261–1279, 2000.
37. A. Bacciotti, "Stabilization by means of state space depending switching rules," *Syst. and Cont. Letter*, Vol. 53, pp. 195–201, 2004.
38. V. Jurdjevic and J. P. Quinn, "Controllability and Stability," *J. Diff. Equation*, Vol. 28, No.3, pp 381–389, 1978.
39. A. Bacciotti and F. Ceragioli, "Closed loop stabilization of planar bilinear switched systems," *Int. J. of Cont.*, Vol. 79, No. 1, pp. 14–23, 2006.
40. H. Lin and P.J. Antasklis, "Switching Stabilizablility for Continuous-Time Uncertain Switched Linear Systems," *IEEE Trans. on Auto. Cont.*, Vol. 52, No. 4,

pp. 633–646, 2007.

41. V. I. Utkin and K. D. Young, “Methods for constructing discontinuity planes in multidimensional variable structure systems,” *Automation Remote Cont.*, Vol. 39, pp. 1466–1470, 1979.
42. O. M. E. Elghezawi, A. S. I. Zinober, and S. A. Billings, “Alalysis and design of variable structure systems using a geometric approach,” *Int. J. of Cont.*, Vol. 38, pp. 657–671, 1983.
43. W. C. Su, S. V. Drakunov, and Ü. Özgüner, “Constructing discontinuity surface for variable structure system: a Lyapunov approach,” *Automatica*, Vol. 32, pp. 925–928, 1996.
44. S. Banerjee and G.C. Verghese, *Nonlinear Phenomena in Power Electronics: Attractors, Bifurcations, Chaos, and Nonlinear Control*, Ch. 8, IEEE Press, New York, 2001.
45. V. S. C. Raviraj and P. C. Sen, “Comparative study of proportional-integral, sliding mode, and fuzzy logic controller for power converters,” *IEEE Trans. Ind. Applicat.*, Vol. 33, No. 2, pp. 518–524, 1997.
46. Jeang-Lin Chang and Yon-Ping Chen, “Sliding Vector Design Based on the Pole-Assignment Method,” *Asian J. of Cont.*, Vol. 2, No. 1, pp. 10–15, 2000.

VITA

學經歷資料

姓名：蔡建峰

性別：男

生日：民國 65 年 11 月 28 號

出生地：高雄市

論文題目：

中文：Bang-Bang 順滑控制在切換式電源轉換器之設計

英文：Bang-Bang Sliding Mode Control in Switching Power Converters

學歷

1. 民國 84 年 9 月~民國 88 年 6 月　國立清華大學動力機械工程學系

2. 民國 88 年 9 月~民國 90 年 6 月　國立清華大學動力機械工程學系碩士班

3. 民國 90 年 9 月~民國 96 年 10 月　國立交通大學電機與控制工程學系博士班

PUBLICATION LIST

著作目錄

姓名 ： 蔡建峰 (Jian-Feng Tsai)

期刊論文:

[1] Jian-Feng Tsai, Yon-Ping Chen, “Design and Performance Analysis of an Axial-Flux Disk-Type Switched Reluctance Motor for Hybrid Scooters,” *JSME, Series C*, vol. 49, No. 3, pp. 882-889, Sept. 2006.

[2] Jian-Feng Tsai, Yon-Ping Chen, “Sliding Mode Control and Stability Analysis of Buck DC-DC Converter,” *International Journal of Electronics*, Vol. 94, No. 3, pp. 209-222, March 2007.

研討會 ：

[1] 蔡建峰，陳永平, 2004, “Stability Analysis and Sliding Mode Control of Buck Dc-Dc Converter with Parasitic Resistance,” *中華民國自動控制研討會*, 2004.

[2] Y.-H. Hung, J.-F. Tsai, and C.-T. Hsu, “An Optimized on-Line Control Strategy for A PEM Fuel Cell Battery Hybrid Electric Scooter”, *8th International Symposium on Advanced Vehicle Control*, Taipei, 2006.